Inorganic Chemistry

Article

pubs.acs.org/IC

Lanthanide Germanate Cluster Organic Frameworks Based on $\{Ln_8Ge_{12}\}$ Clusters: From One-Dimensional Chains to Two-Dimensional Layers and Three-Dimensional Frameworks

Lei-Lei Li,[†,#] Gao-Juan Cao,[∥,#] Jun-Wei Zhao,[*,‡] Huan He,[†] Bai-Feng Yang,[†] and Guo-Yu Yang[*,†,§]

[†]MOE Key Laboratory of Cluster Science, School of Chemistry, Beijing Institute of Technology, Beijing 100081, China

[‡]Henan Key Laboratory of Polyoxometalate Chemistry, College of Chemistry and Chemical Engineering, Henan University, Kaifeng, Henan 475004, China

[§]Department of Chemistry and Key Laboratory for Preparation and Application of Ordered Structural Materials of Guangdong Province Shantou University, Shantou, Guangdong 515063, China

[∥]Department of Applied Chemistry, School of Life Science Fujian Agriculture and Forestry University, Fuzhou, Fujian 350002, China

Supporting Information

ABSTRACT: Under hydrothermal conditions, six series of novel lanthanide (Ln) organogermanates (LnGs) $[Ln_8Ge_{12}(\mu_3\text{-}O)_{24}E_{12}(H_2O)_{16}]\cdot 14H_2O$ (Ln^{3+} = Pr^{3+}, **1**; Nd^{3+}, **2**; Sm^{3+}, **3**; Eu^{3+}, **4**; Gd^{3+}, **5**; one-dimensional (1-D) LnG cluster organic chain (LnGCOC)), $\{[Nd_8Ge_{12}(\mu_3\text{-}O)_{24}E_{12}(H_2O)_{10}](\mu_2\text{-}H_2O)_2[Nd_8Ge_{12}(\mu_3\text{-}O)_{24}E_{12}(H_2O)_{16}]\}\cdot 18H_2O$ (**6**, two-dimensional (2-D) planar LnG cluster organic layer (LnGCOL)), $\{[Ln_2GeE(HO)_2O(H_2O)(CH_3COO)_2(CO_3)]_2[Ln_8Ge_{12}E_{12}(\mu_3\text{-}O)_{24}(H_2O)_{10}]\}\cdot 6H_2O$ (Ln^{3+} = Pr^{3+}, **7**; Nd^{3+}, **8**; 2-D wave-shaped LnGCOL), $[TbGeE(HO)_2O(H_2O)(pca)]_2[Tb_8Ge_{12}E_{12}(\mu_3\text{-}O)_{24}(H_2O)_8]\cdot 10H_2O$ (**9**, three-dimensional (3-D) LnG cluster organic framework (LnGCOF)), $\{([Nd(pza)_2(H_2O)_2]_2[Nd_8Ge_{12}E_{12}(\mu_3\text{-}O)_{24}(H_2O)_{12}])([Nd(pza)_2]_2[Nd_8Ge_{12}E_{12}(Hpza)_2(\mu_3\text{-}O)_{24}(H_2O)_{10}])\}\cdot 4OH\cdot 14H_2O$ (**10**, 3-D LnGCOF), $\{[Nd_8Ge_{12}E_{12}(\mu_3\text{-}O)_{24}(H_2O)_{10}][Nd(pca)(pda)(H_2O)]_2\}\cdot 12H_2O$ (**11**, 3-D LnGCOF) and $\{[Nd_8Ge_{12}E_{12}(\mu_3\text{-}O)_{24}(H_2O)_{10}][Nd(pza)(pda)(H_2O)]_2\}\cdot 12H_2O$ (**12**, 3-D LnGCOF) (Hpca = 2-picolinic acid, H_2pda = 2,6-pyridinedicarboxylic acid, Hpza = 2-pyrazinecarboxylic acid) were prepared by introducing the second auxiliary ligands into the organogermanate−lanthanide−oxide reaction system. The obtainment of these LnGs realized the utilization of the second auxiliary ligands inducing the assembly from 1-D LnGCOCs to 2-D LnGCOLs and 3-D LnGCOFs based on LnG cluster (LnGC) $\{Ln_8Ge_{12}E_{12}(\mu_3\text{-}O)_{24}(H_2O)_{16}\}$-($\{Ln_8Ge_{12}\}$) units and Ln−organic complexes or organic ligand connectors. It should be noted that the well-organized structural constructions of **1**−**12** can be visualized as the gradual replacement of active water sites located at equatorial and polar positions on the hypothetical $[Ln_8Ge_{12}(\mu_3\text{-}O)_{24}E_{12}(H_2O)_{18}]$ LnGC core with oxygen or nitrogen atoms from organic ligands. The solid-state luminescent properties of **2**, **3**, **4**, **6**, and **8**−**12** have been investigated at room temperature.

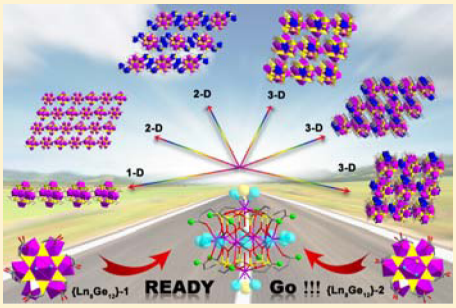

INTRODUCTION

The design and synthesis of functional microporous materials with interesting structural features and potential applications in catalysis, absorption, separation, and ion-exchange, are of great interest and hold a significant position in the discovery and utilization of new materials.[1] Because of high thermal stability and good optical transparency, IIIA and IVA main-group elements are usually selected as excellent candidates for constructing porous zeolite materials.[2] For example, zeolites with tetrahedrally coordinated Si, Al, or P framework elements are one of the most widely applied catalysts in industry and have become successful as catalysts in petroleum refining and organic synthesis in the production of fine chemicals.[1a] Actually, since the mysterious veil of the first three germanate frameworks with occluded ethylenediamine, 1,3-propylenediamine, or tetramethylammonium hydroxide were discovered by Xu et al. in 1991,[3] germanates have attracted increasing attention and have developed as an important branch of microporous materials because the most obvious advantage of introducing germanium to microporous structures is that the Ge−O−Ge angles (~130°) are smaller than the Si−O−Si angles (~145°), which is necessary to construct framework structures with 3- and 4-rings.[4a] It has proved that germanium can form both 3-rings and 4-rings and has a propensity to build double 4-rings through oxygen atoms.[4b−g] Furthermore, the flexible coordination geometries (GeO_4 tetrahedra, GeO_5 trigonal bipyramids, and GeO_6 octahedra) of germanium contribute to the structural diversity of germanate clusters (Figure S1), such as Ge_7X_{19} (Ge_7), Ge_8X_{20-24} (Ge_8), Ge_9X_{26-m} (Ge_9, m = 0−1), $Ge_{10}X_{27/28}$ (Ge_{10}), $Ni@Ge_{14}X_{30}$ ($Ni@Ge_{14}$) (X = O, OH, F),[5−10] which can further function as structural building units (SBUs) to construct novel germanate frameworks. For instance, the 2-D layer germanate ASU-19 with 8-

Received: March 25, 2016
Published: May 24, 2016

DOI: 10.1021/acs.inorgchem.6b00754
Inorg. Chem. 2016, 55, 5671−5683

and 12-ring channels is all constructed from typical $\{Ge_7\}$ SBUs;[5b] two 3-D open frameworks $[GeO_2]_{10}\cdot C_2N_2H_8\cdot H_2O$ and $[GeO_2]_{10}\cdot C_3N_2H_{10}\cdot H_2O$ are made by $\{Ge_8\}$ double four-ring units;[11] an intriguing 3-D FDU-4 with large 24-ring channels is built from $\{Ge_9\}$ SBUs;[12] SU-M with extra-large 30-ring channels is based on $\{Ge_{10}\}$ SBUs;[8b] and the porous materials FJ−1a/FJ−1b containing Ge−Ni−Ge linkers are constructed from chiral $\{Ni@Ge_{14}\}$ clusters.[9]

Introducing heteroatoms into the germanate system has been proven to be an effective strategy for preparing novel germanate materials.[13−15] To date, although numerous germanate architectures incorporating main-group elements (B,[13a−d] Al,[13e,f] Si,[13g] In,[13h,2] Sb[13i]) and transition-metal elements (V,[14a] Cu,[14b] Zn,[14c] Zr,[14d−f] Nb,[14g,h] Cd[14i]) have been obtained, reports on lanthanide (Ln) encapsulated germanates remain largely unexplored mainly because of the incompatibility of solubility conditions of traditional germanium resource (GeO_2) and lanthanide oxide (Ln_xO_y).[15] That is, acidic and basic solutions are favorable for Ln_xO_y and GeO_2, respectively. However, the high coordination number, flexible coordination geometry, and strong oxophilicity of Ln ions allow building large SBUs to assemble Ln encapsulated germanate aggregates or open frameworks. Moreover, the narrow emission bands and high color purity of Ln ions can endow Ln-based materials with special optical properties involving light emitting diodes, sensory probes, and fluorescent tubes.[16] On the other hand, a large number of useful Ln encapsulated silicates with high thermal stability, uniform microporosity, and potential applications in optical materials and fast alkali-ion conductors[17] enlighten and drive us to explore novel Ln germanates with potential applications. To our knowledge, relevant investigations on Ln organogermanates (LnGs) have been much less made.[15] As a result, our great attempts have been made to this domain by substituting germanium dioxide with soluble germanium alkoxides in the acidic condition, replacing Ln_xO_y with Ln salts in the basic condition and reactions of Ln salts and germanium alkoxides in the acidic solution. Finally, we failed due to the hydrolysis of Ln ions into nondissolving phases in the basic solution or the very poor crystallization of products. Upon the analysis of the above-mentioned unsuccessful experimental results and the enlightenment of our previously reported Ln−O cluster organic frameworks in which the formation of Ln−O cluster SBUs can be directed by carboxyl groups of organic ligands,[18] we selected bis-(carboxyethl germanium sesquioxide) $(HOOCCH_2CH_2)_2Ge_2O_3$ ($H_2E_2Ge_2O_3$, E = $-CH_2CH_2COO^-$) (Scheme 1) with two carboxylic groups[19] to replace GeO_2 to make novel LnGs with fascinating structures and properties under mild hydrothermal conditions based on the following considerations: (a) $H_2E_2Ge_2O_3$ with two hydrophilic carboxyl groups has a good solubility in aqueous solution and the acid environment provided by $H_2E_2Ge_2O_3$ facilitate to dissolve Ln_xO_y to the reaction system. (b) Two types of functional groups on $H_2E_2Ge_2O_3$ can be utilized as active sites for constructing organic−inorganic hybrid LnGs based on $\{Ln_xGe_y\}$ cluster SBUs by Ln−O interactions. Specifically, the opening of two Ge═O bonds in the Ge_2O_3 (O═Ge−O−Ge═O) core can not only polymerize to form Ge−O clusters or Ge−O chains, but also provide highly active oxygen atoms to capture Ln ions for the formation of $\{Ln_xGe_y\}$ SBUs. Two carboxyl groups on $H_2E_2Ge_2O_3$ can serve as multidentate chelating sites to arrest Ln ions, forming expanded frameworks based on in situ formed $\{Ln_xGe_y\}$ SBUs. (c) The skeleton of $H_2E_2Ge_2O_3$ can be broken into highly active germanium sources to combine with Ln ions, giving rise to the assembly of unprecedented $\{Ln_xGe_y\}$ cluster SBUs or frameworks. Following these ideas, six classes of novel lanthanide organogermanates (LnGs) $[Ln_8Ge_{12}(\mu_3\text{-}O)_{24}E_{12}(H_2O)_{16}]\cdot 14H_2O$ (Ln^{3+} = Pr^{3+}, **1**; Nd^{3+}, **2**; Sm^{3+}, **3**; Eu^{3+}, **4**; Gd^{3+}, **5**; 1-D LnG cluster organic chain (LnGCOC)), $\{[Nd_8Ge_{12}(\mu_3\text{-}O)_{24}E_{12}(H_2O)_{10}](\mu_2\text{-}H_2O)_2[Nd_8Ge_{12}(\mu_3\text{-}O)_{24}E_{12}(H_2O)_{16}]\}\cdot 18H_2O$ (**6**, 2-D planar LnG cluster organic layer (LnGCOL)), $\{[Ln_2GeE(HO)_2O(H_2O)(CH_3COO)_2(CO_3)]_2[Ln_8Ge_{12}E_{12}(\mu_3\text{-}O)_{24}(H_2O)_{10}]\}\cdot 6H_2O$ (Ln^{3+} = Pr^{3+}, **7**; Nd^{3+}, **8**; 2-D wave-shaped LnGCOL), $[TbGeE(HO)_2O(H_2O)(pca)]_2[Tb_8Ge_{12}E_{12}(\mu_3\text{-}O)_{24}(H_2O)_8]\cdot 10\ H_2O$ (**9**, 3-D LnG cluster organic framework (LnGCOF)), $\{([Nd(pza)_2(H_2O)_2]_2[Nd_8Ge_{12}E_{12}(\mu_3\text{-}O)_{24}(H_2O)_{12}])([Nd(pza)_2]_2[Nd_8Ge_{12}E_{12}(Hpza)_2(\mu_3\text{-}O)_{24}(H_2O)_{10}])\}\cdot 4OH\cdot 14H_2O$ (**10**, 3-D LnGCOF), $\{[Nd_8Ge_{12}E_{12}(\mu_3\text{-}O)_{24}(H_2O)_{10}][Nd(pca)(pda)(H_2O)]_2\}\cdot 12H_2O$ (**11**, 3-D LnGCOF) and $\{[Nd_8Ge_{12}E_{12}(\mu_3\text{-}O)_{24}(H_2O)_{10}][Nd(pza)(pda)(H_2O)]_2\}\cdot 12H_2O$ (**12**, 3-D LnGCOF) (Hpca = 2-picolinic acid, H_2pda = 2,6-pyridinedicarboxylic acid, Hpza = 2-pyrazinecarboxylic acid) were synthesized under hydrothermal conditions. These LnGCOCs/COLs/COFs have been structurally characterized by elemental analyses, IR spectra, powder X-ray diffraction (PXRD), single-crystal X-ray diffraction and thermogravimetric (TG) analyses. This in situ reaction substitution strategy under hydrothermal conditions not only provides an effectual methodology of constructing novel LnGC-based materials but also opens a new avenue for discovering other metal germanate functional materials. The photoluminescence emission spectra of **2**, **3**, **4**, **6**, and **8**−**12** reveal the characteristic emission bands resulting from Ln cations.

Scheme 1. (a) The Structure of $H_2E_2Ge_2O_3$. (b) The Potential Coordination Sites of $E_2Ge_2O_5^{6-}$ Accompanying the Opening of Two Ge═O Bonds and the Insertion of Two Additional Oxygen Atoms. (c) The Potential Coordination Sites of the Resulting $EGeO_3^{4-}$ Derived from the Opening of the Ge−O Bond and the Insertion of One Additional Oxygen Atom

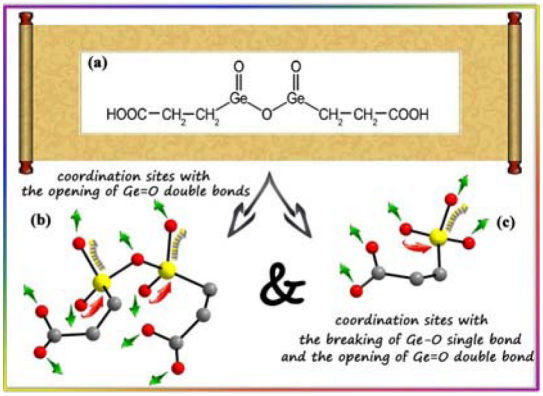

EXPERIMENTAL SECTION

Materials and Methods. All chemicals were purchased commercially and used without further purification. PXRD data were collected on a Bruker D8 Advance diffractometer with Cu Kα radiation (λ = 1.5406 Å). C, H, and N elemental analyses were performed on a Euro EA 3000 CHNS/O analyzer. IR spectra were recorded on a Smart Omin-Transmission spectrophotometer with KBr pellets in the range of 4000−400 cm^{-1}. TG analyses were carried out on a Mettler TGA/SDTA 851 thermal analyzer in the temperature range of 25−

DOI: 10.1021/acs.inorgchem.6b00754
Inorg. Chem. 2016, 55, 5671−5683

Table 1. Crystallographic Data and Structure Refinements for 1−12

	1	2	3	4	5	6
formula	$C_{36}H_{108}O_{78}Ge_{12}Pr_8$	$C_{36}H_{108}O_{78}Ge_{12}Nd_8$	$C_{36}H_{108}O_{78}Ge_{12}Sm_8$	$C_{36}H_{108}O_{78}Ge_{12}Eu_8$	$C_{36}H_{108}O_{78}Ge_{12}Gd_8$	$C_{72}H_{188}O_{142}Ge_{24}Nd_{16}$
fw	3787.58	3814.22	3863.10	3875.98	3918.30	7376.22
crystal system	monoclinic	monoclinic	monoclinic	monoclinic	monoclinic	triclinic
space group	$P2_1/n$	$P2_1/n$	$P2_1/n$	$P2_1/n$	$P2_1/n$	$P\bar{1}$
a, Å	13.4082(3)	13.4063(4)	13.3203(4)	13.2863(2)	13.2654(2)	15.1938(14)
b, Å	23.7792(6)	23.7170(7)	23.4821(7)	23.4503(4)	23.3935(4)	16.548(2)
c, Å	16.0076(4)	16.0178(6)	15.9302(5)	15.9547(3)	15.9730(3)	19.731(2)
α, deg	90	90	90	90	90	107.175(5)
β, deg	100.704(3)	100.7900	100.916(3)	100.913(2)	100.845(2)	91.052(3)
γ, deg	90	90	90	90	90	97.001(6)
V, Å^3	5015.0(2)	5002.9(3)	4892.6(3)	4881.07(14)	4868.28(14)	4696.6(9)
Z	2	2	2	2	2	1
D_c, g cm^{-3}	2.508	2.532	2.622	2.637	2.673	2.608
T, K	293(2)	293(2)	293(2)	293(2)	293(2)	293(2)
$F(000)$	3608	3624	3656	3672	3688	3484
μ, mm^{-1}	7.449	7.723	8.453	8.800	9.119	8.216
Reflections collected/ unique	26396/8804	20068/8410	25877/8591	33515/10894	31939/8557	36809/21289
R_{int}	0.0349	0.0756	0.0923	0.0397	0.0573	0.0947
GOF on F^2	1.047	1.025	1.012	1.033	1.053	1.062
R_1, wR_2 ($I > 2\sigma(I)$)[a]	0.0413, 0.0983	0.0619, 0.1216	0.0708, 0.1858	0.0397, 0.0896	0.0451, 0.1152	0.1167, 0.2623
R_1, wR_2 (all data)	0.0517, 0.1061	0.1068, 0.1364	0.0785, 0.1945	0.0563, 0.0976	0.0532, 0.1241	0.1858, 0.3361

	7	8	9	10	11	12
formula	$C_{52}H_{108}O_{90}Ge_{14}Pr_{12}$	$C_{52}H_{108}O_{90}Ge_{14}Nd_{12}$	$C_{54}H_{108}N_2O_{82}Ge_{14}Tb_{10}$	$C_{122}H_{212}N_{20}O_{160}Ge_{24}Nd_{20}$	$C_{62}H_{110}N_4O_{84}Ge_{12}Nd_{10}$	$C_{60}H_{108}N_6O_{84}Ge_{12}Nd_{10}$
fw	4880.56	4920.52	4702.88	9146.08	4569.02	4571.00
crystal system	orthorhombic	orthorhombic	monoclinic	triclinic	monoclinic	monoclinic
space group	*Pbca*	*Pbca*	$P2_1/c$	$P\bar{1}$	$P2_1/n$	$P2_1/n$
a, Å	17.7742(3)	17.7374(3)	17.660(5)	15.9088(19)	16.3388(8)	16.425(6)
b, Å	25.4947(4)	25.2703(4)	20.309(5)	16.755(2)	18.94026)	18.842(6)
c, Å	27.3526(6)	27.2582(4)	17.565(5)	22.433(3)	19.5016(8)	19.184(7)
α, deg	90	90	90	87.050(4)	90	90
β, deg	90	90	115.926(4)	84.278(3)	107.165(3)	106.542(5)
γ, deg	90	90	90	83.494(2)	90	90
V, Å^3	12394.8(4)	12217.9(3)	5666(3)	5906.5(12)	5764.4(4)	5692(3)
Z	4	4	2	1	2	2
D_c, g cm^{-3}	2.615	2.675	2.754	2.571	2.632	2.667
T, K	293(2)	293(2)	293(2)	293(2)	293(2)	293(2)
$F(000)$	9184	9232	4392	4332	4332	4332
μ, mm^{-1}	8.059	8.490	9.909	7.420	7.604	7.701
reflections collected/ unique	43085/10897	42182/10687	43765/12759	46138/26533	41959/12980	41959/12980
R_{int}	0.0318	0.0517	0.0532	0.0285	0.0387	0.0387
GOF on F^2	1.013	1.055	1.078	1.081	1.028	1.078
R_1, wR_2 ($I > 2\sigma(I)$)[a]	0.0307, 0.0754	0.0711, 0.1800	0.0547, 0.1355	0.0351, 0.0985	0.0371, 0.0874	0.0371, 0.0871
R_1, wR_2 (all data)	0.0395, 0.0804	0.0806, 0.1864	0.0728, 0.1504	0.0449, 0.1152	0.0492, 0.0973	0.0492, 0.0972

1000 °C in air atmosphere with a heating rate of 10 °C min^{-1}. Luminescence measurements were performed in the solid state at room temperature with an Edinburgh FLS920 fluorescence spectrometer. During the course of the excitation and emission spectra, the 850 nm optical filter was used for **2**, **6**, **8**, **10**, **11**, and **12**, the 495 nm optical filter was used for **3** and **4**, and the 455 nm optical filter was used for **9**.

Syntheses of 1−5. $H_2E_2Ge_2O_3$ (0.084 g, 0.247 mmol) and Ln_xO_y [Pr_6O_{11} (0.085 g, 0.083 mmol) for **1**, Nd_2O_3 (0.084 g, 0.253 mmol) for **2**, Sm_2O_3 (0.087 g, 0.249 mmol) for **3**, Eu_2O_3 (0.088 g, 0.250 mmol) for **4** and Gd_2O_3 (0.091 g, 0.251 mmol) for **5**] were suspended in water (10 mL, 556 mmol) and stirred for 2 h (pH_i = 3). The resulting mixture was sealed in a 40 mL Teflon-lined steel autoclave, kept at 140 °C for 7 days, and cooled to room temperature (pH_f = 7). Block (green for **1**, pink for **2** and colorless for **3**−**5**) crystals of **1**−**5** were obtained by filtering, washed with distilled water, and then dried in air at ambient temperature. Yield: ca. 55%, 58%, 52%, 45%, and 32% for **1**−**5**, respectively (based on $H_2E_2Ge_2O_3$). Elemental analyses (%) calcd. for **1**: C 11.41, H 2.87; for **2**: C 11.33, H 2.85; for **3**: C 11.19, H 2.82; for **4**: C 11.15, H 2.81; for 5: C 11.03, H 2.78. Found: C 11.33, H 2.94 for **1**; C 11.21, H 2.79 for **2**; C 11.11, H 2.89 for **3**; C 11.26, H 2.91 for **4**; C 11.15, H 2.85 for **5**. IR (KBr, cm^{-1}): 3409 (br), 2932 (w), 1583 (vs), 1431 (m), 1397 (m), 1300 (w), 1159 (w), 764 (vs), 605 (w), 526 (m) (Figure S2 in the Supporting Information).

Synthesis of 6. The synthetic process of **6** is similar to **2** except that the amount of Nd_2O_3 was changed to 0.090 g (0.267 mmol) and pyridine (1 mL, 10.923 mmol) was added (pH_i = 7, pH_f = 8). Prismatic pink crystals were isolated. Yield: ca. 45% (based on

DOI: 10.1021/acs.inorgchem.6b00754
Inorg. Chem. 2016, 55, 5671−5683

$H_2E_2Ge_2O_3$). Elemental analyses (%) calcd. for **6**: C 11.72, H 2.57. Found: C 11.68, H 2.53. IR (KBr, cm^{-1}): 3420 (br), 2940 (w), 1577 (vs), 1431 (m), 1390 (m), 1287 (w), 1151 (m), 770 (vs), 611 (w), 526 (m).

Syntheses of 7 and 8. The synthetic processes of **7** and **8** are similar to **1** and **2**, respectively, except that propanedioic acid (0.052 g, 0.050 mmol) was added (pH_i = 2, pH_f = 7). Green (**7**) and pink (**8**) prismatic crystals were obtained. Yield: *ca.* 48% and 37% for **7** and **8**, respectively (based on $H_2E_2Ge_2O_3$). Elemental analysis (%) calcd. for **7**: C 12.80, H 2.23; for **8**: C 12.69, H 2.12. Found: C 12.77, H 2.20 for **7**; C 12.66, H 2.08 for **8**. IR (KBr, cm^{-1}): 3414 (br), 2950 (w), 1607 (vs), 1444 (m), 1391 (m), 1298 (w), 1159 (w), 1060 (w), 1020 (w), 771(vs), 711(w), 601(w), 519 (m), 420 (w).

Synthesis of 9. A mixture of $H_2E_2Ge_2O_3$ (0.150 g, 0.442 mmol) and Tb_4O_7 (0.074 g, 0.099 mmol) was stirred in water (10 mL, 556 mmol) for about 5 min, and Hpca (0.124 g, 1.016 mmol) and $HClO_4$ (0.077 g, 0.770 mmol) were added (pH_i = 2). The mixture was stirred for 30 min, sealed in a 40 mL Teflon-lined bomb at 170 °C for 7 days and cooled to room temperature (pH_f = 5). Yellow prismatic crystals of **9** were obtained. Yield: 35% based on $H_2E_2Ge_2O_3$. Elemental analysis (%) calcd. for **9**: C 13.79, H 2.31, N 0.60. Found: C 13.76, H 2.27, N 0.57. IR (KBr, cm^{-1}): 3413 (br), 2944 (w), 1626 (w), 1575 (vs), 1434 (m), 1377(m), 1287(w), 1171(w), 1079 (w), 1035 (m), 780 (vs), 715 (w), 615 (w), 523 (m).

Synthesis of 10. The synthetic process of **10** is similar to **9** except that $H_2E_2Ge_2O_3$, Tb_4O_7 and Hpca were replaced by $H_2E_2Ge_2O_3$ (0.078 g, 0.230 mmol), Nd_2O_3 (0.098 g, 0.291 mmol) and Hpza (0.140 g, 1.014 mmol), respectively (pH_i = 2, pH_f = 5). Yellow prismatic crystals of **9** were obtained. Yield: ca. 56% for **10** (based on $H_2E_2Ge_2O_3$). Elemental analysis (%) calcd. for **10**: C 16.02, H 2.34, N 3.06. Found: C 16.12, H 2.51, N 2.95. IR (KBr, cm^{-1}): 3430 (br), 2955 (w), 1571 (vs), 1423 (m), 1383 (m), 1287 (w), 1165 (w), 1034 (w), 821 (w), 770 (vs), 713 (m), 611 (w), 526 (m).

Syntheses of 11 and 12. The synthetic processes of **11** and **12** are similar to **9** except that $H_2E_2Ge_2O_3$, Tb_4O_7, and Hpca were replaced by $H_2E_2Ge_2O_3$ (0.117 g, 0.345 mmol), Nd_2O_3 (0.100 g, 0.297 mmol), Hpca (0.062 g, 0.508), and H_2pda (0.065 g, 0.389) for **11** (Hpza (0.060 g, 0.483 mmol) and H_2pda (0.046 g, 0.275 mmol) for **12**), respectively (pH_i = 2, pH_f = 5). Pink prismatic crystals of **11** and **12** were isolated. Yield: ca. 42% for **11** and 40% for **12** (based on $H_2E_2Ge_2O_3$). Elemental analysis (%) calcd. for **11**: C 16.30, H 2.43, N 1.22. Found: C 16.21, H 2.35, N 1.14. IR (KBr, cm^{-1}) for **11**: 3421 (br), 2945 (w), 1577 (vs), 1434 (m), 1373 (m), 1304 (w), 1289 (w), 1170 (w), 1044 (w), 768 (vs), 765 (vs), 611 (w), 526 (m). Elemental analysis (%) calcd. for **12**: C, 15.76; H, 2.38; N, 1.84. Found: C, 15.71; H, 2.34; N, 1.80. IR (KBr, cm^{-1}) for **12**: 3434 (br), 2965 (w), 2929 (w), 2849 (w), 1583 (vs), 1436 (m), 1380 (m), 1294 (w), 1258 (w), 1154 (w), 1086 (w), 1051 (w), 1017 (w), 764 (vs), 706 (w), 616 (w), 532 (m).

X-ray Crystallography. Intensity data for **1**−**12** were collected on a Gemini A Ultra diffractometer with a Atlas CCD area detector with graphite monochromated Mo Kα (λ = 0.71073 Å). Their structures were determined and the heavy atoms were found by direct methods using the SHELXTL-97 program package.[20] The remaining atoms were found from successive full-matrix least-squares refinements on F^2 and Fourier syntheses. Routine Lorentz polarization and the empirical absorption correction were applied to intensity data. All non-hydrogen atoms were refined anisotropically except for some oxygen and carbon atoms and water molecules. All hydrogen atoms attached to carbon atoms were geometrically placed and refined isotropically as a riding model using the default SHELXTL parameters. No hydrogen atoms associated with water molecules were located from the difference Fourier map. Notably, some C and O atoms from E groups in **1**−**5** and the $Tb2^{3+}$ ion in **9** are disordered over two positions. Crystallographic data and structural refinements for **1**−**12** are summarized in Table 1. Crystallographic data for this paper have been deposited in the Cambridge Crystallographic Data Centre with CCDC 1442692−1443699, 1443703, and 1443700−1443702 for **1**−**12**, respectively. These data can be obtained free of charge from The Cambridge Crystallographic Data Centre via www.ccdc.cam.ac.uk/data_request/cif.

RESULTS AND DISCUSSION

Structures of 1-D LnGCOCs of 1−5. X-ray diffraction reveals that isomorphs **1**−**5** $[Ln_8Ge_{12}(\mu_3\text{-}O)_{24}E_{12}(H_2O)_{16}]\cdot 14H_2O$ (Ln^{3+} = Pr^{3+}, **1**; Nd^{3+}, **2**; Sm^{3+}, **3**; Eu^{3+}, **4**; Gd^{3+}, **5**) crystallize in monoclinic space group $P2_1/n$ and display novel 1-D LnGCOC alignment constructed from cage-like $\{Ln_8Ge_{12}E_{12}(\mu_3\text{-}O)_{24}(H_2O)_{16}\}(\{Ln_8Ge_{12}\})$ hybrid LnGCs via double carboxyl connectors from E groups. Therefore, only the structure of **1** will be discussed below. In the structure of **1**, the most interesting is the $\{Ln_8Ge_{12}\}$ LnGC SBU. The neutral cage-like $\{Pr_8Ge_{12}\}$-**1** SBU (Figure 1a) consists of two

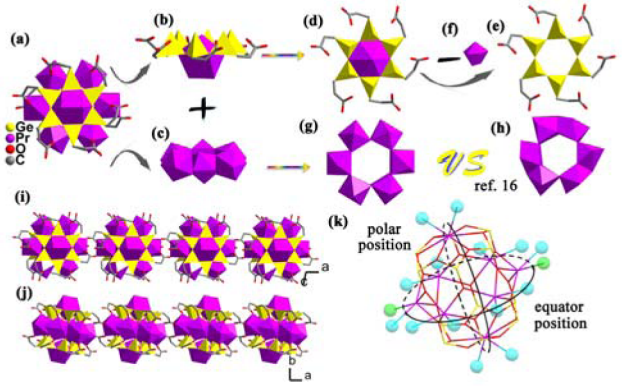

Figure 1. (a) Top view of the $\{Pr_8Ge_{12}\}$-**1** SBU. (b) Side view of the monocapped hexagon $\{PrGe_6\}$ subunit in **1**. (c) Side view of the Pr_6 ring with six edge-sharing $\{PrO_8\}$ units in **1**. (d) Top view of the monocapped hexagon $\{PrGe_6\}$ subunit in **1**. (e) Top views of the wheel-shaped Ge_6 ring in **1**. (f) The capped nine-coordinate $\{PrO_9\}$ irregular polyhedron in **1**. (g) Top view of the Pr_6 ring with six edge-sharing $\{PrO_8\}$ units in **1**. (h) The Pr_6 ring in **FJ-19** with three edge-sharing $\{Pr_2\}$ dimers. (i) The 1-D chain alignment of **1** viewed along the *b* axis. (j) The simplified mode of the 1-D chain with double E groups. (k) Highlight of the active sites (green balls) and potential active sites in Pr^{3+} centers (turquoise balls) in the $\{Pr_8Ge_{12}\}$-1 SBU.

equivalently related $\{Pr_4Ge_6\}$ half-units (Figure S3a in the Supporting Information) by an inversion center with atomic coordinate of (0.5, 0.5, 0.5). Alternatively, the centrosymmetrical $\{Pr_8Ge_{12}\}$-**1** SBU can be also visualized as two monocapped hexagon $\{PrGe_6\}$ subunits (Figure 1b) sandwiching one hexagon $\{Pr_6\}$ ring (Figure 1c) through 12 μ_2-O_{COO} atoms from 12 E groups and 12 exotic μ_3-O_e atoms originating from the opening of 12 Ge=O double bonds (Figure S3b in the Supporting Information). The monocapped hexagon $\{PrGe_6\}$ subunit (Figure 1d) is made up of a six-membered Ge_6 ring (Figure 1e) capped by a $\{Pr4O_9\}$ irregular dodecahedron (Figure 1f) via coordination of six μ_3-O atoms to the Pr^{3+} ion (Figure S3c in the Supporting Information). Three μ_3-O atoms are from the bridging atoms of O=Ge−O−Ge=O groups in three $E_2Ge_2O_3^{2-}$ ligands, and the remaining three μ_3-O atoms come from the terminal atoms of O=Ge−O−Ge=O groups in three $E_2Ge_2O_3^{2-}$ ligands. It is worth emphasizing that, under hydrothermal reactions, two Ge=O double bonds of O=Ge−O−Ge=O groups in organogermanium source ($E_2Ge_2O_3^{2-}$) are opened for the polymerization of Ge_6 ring, while six E units flexibly radiate out of the periphery of the Ge_6 ring giving rise to a wheel-shaped hybrid cluster (Figure S3e in the Supporting Information). In the six-

DOI: 10.1021/acs.inorgchem.6b00754
Inorg. Chem. 2016, 55, 5671−5683

membered Ge_6 ring, each Ge center binds one C atom and two O atoms from one $E_2Ge_2O_3^{2-}$ ligand and one O atom from the other $E_2Ge_2O_3^{2-}$ ligand to complete the tetrahedral coordination sphere (Figure S4a–c in Supporting Information), and then each $\{GeO_3C\}$ tetrahedron combines with two neighboring identical $\{GeO_3C\}$ tetrahedra via the corner-sharing fashion to construct the wheel-shaped Ge_6 ring. More interestingly, in the formation of $\{Pr_8Ge_{12}\}$-**1** SBU, the Ge_6 ring plays the structure-directing function. On one hand, the Ge_6 ring exerts its hexadentate ability to arrest the capped nine-coordinate $\{Pr4O_9\}$ irregular dodecahedron [Pr4–O: 2.510(6)–2.711(5) Å], and the remaining three coordination sites of $\{Pr4O_9\}$ dodecahedron are accomplished by three water ligands [Pr4–O: 2.418(8)–2.547(6) Å] (Figure S4d–f in Supporting Information). On the other hand, two face-to-face Ge_6 rings anchor a hexagon Pr_6 ring via 12 apical μ_3-O atoms of $\{GeO_3C\}$ tetrahedra and 12 inflexed carboxyl O atoms from 12 E groups, respectively. All the Pr^{3+} centers in the Pr_6 ring exhibit eight-coordinate distorted bicapped trigonal prism geometries [Pr–O: 2.373(5)–2.659(14) Å] (Figure S4g–o in the Supporting Information). A closer examination reveals that 24 O_{coo} atoms of E units in two Ge_6 rings can be classified into three types according to their coordination functions: 12 inflexed O_{COO} atoms link back to the Pr_6 ring, two extrovertive O_{COO} atoms work as linkers to extend the 1-D structure of **1** and 10 extrovertive free O_{COO} atoms (Figure S5 in the Supporting Information). As expected, the O active sites of Ge_2O_3 cores and carboxyl groups in $E_2Ge_2O_3^{2-}$ moieties play an important role in chelating Pr^{3+} ions in the construction of $\{Pr_8Ge_{12}\}$-**1** SBUs. The Ge_6 rings and Pr_6 ring show a staggered alignment mode (Figure S6a-b in the Supporting Information). Although the corresponding Ge centers in the upper and lower Ge_6 rings almost are mirror-symmetrical in $\{Pr_8Ge_{12}\}$-**1** SBU, steric hindrance in the formation of the 1-D chain leads to the misalignment of the corresponding two bridging E groups (Figure S6c in the Supporting Information). Most intriguingly, the hexagon-shaped Pr_6 ring with six edge-sharing $\{PrO_8\}$ units (Figure 1g) is apparently distinct from the Nd_6 ring observed in **FJ-19** where every two Nd^{3+} ions are face-sharing by three μ_3-O atoms to generate a dimeric Nd_2 unit and then three dimeric Nd_2 units are further connected by edge-sharing mode constructing the Nd_6 ring (Figure 1h).[15]

Furthermore, the monocapped Nd^{3+} center in **FJ-19** displays the eight-coordinate hexagonal bipyramid geometry,[15] which is different from the nine-coordinate irregular dodecahedron of the monocapped Pr^{3+} center **1**. The most striking structural feature of **1** is that adjacent $\{Pr_8Ge_{12}\}$-**1** SBUs are interconnected together by double carboxyl connectors from E groups into the 1-D LnGCOCs (Figure 1i,j), which is unobserved among previously reported LnGCOFs.[15] It can been clearly seen that the $Pr1^{3+}$, $Pr1A^{3+}$, $Pr3^{3+}$, or $Pr3A^{3+}$ ion located in the equatorial position in $\{Pr_8Ge_{12}\}$-**1** SBU has two water ligands, whereas $Pr2^{3+}$ or $Pr2A^{3+}$ ion in the equatorial position only possesses a water ligand (Figure 1k). Upon close inspection, the formation of 1-D LnGCOC can be regarded as a self-polymerization of hypothetical $[Pr_8Ge_{12}(\mu_3\text{-}O)_{24}E_{12}(H_2O)_{18}]$ SBUs by substituting one water ligand on $Pr2^{3+}$ and $Pr2A^{3+}$ ions with O_{COO} atoms from E groups, which indicates that water ligands on the hypothetical $[Pr_8Ge_{12}(\mu_3\text{-}O)_{24}E_{12}(H_2O)_{18}]$ SBU are active sites and can be replaced by extraneous O atoms of organic ligands to construct extended architectures.

Structure of the 2-D LnGCOL of 6. As illustrated in Figure 2a, two kinds of $[Nd_8Ge_{12}(\mu_3\text{-}O)_{24}E_{12}(H_2O)_{10}]$

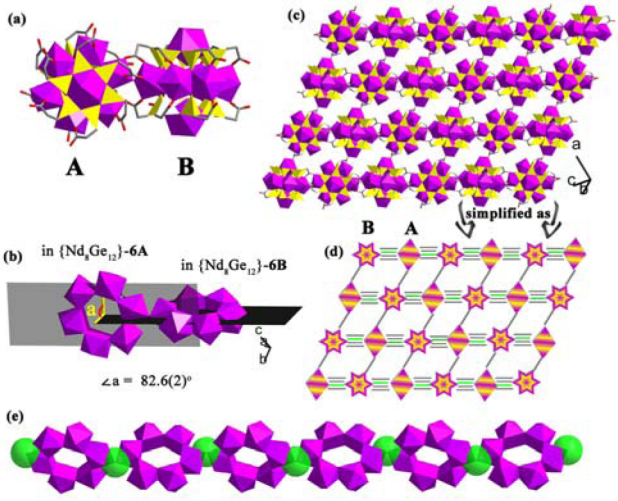

Figure 2. (a) The structure of $\{Nd_{16}Ge_{24}\}$-**6** SBU with $\{Nd_8Ge_{12}\}$-**6A** and $\{Nd_8Ge_{12}\}$-**6B** subunits in different spatial orientations. Symmetric codes: A: $1-x, 1-y, 1-z$; B: $-x, -y, -z$. (b) The dihedral angle of two Nd_6 rings in $\{Nd_8Ge_{12}\}$-**6A** and $\{Nd_8Ge_{12}\}$-**6B** subunits. (c) View of the 2-D layer of **6**. (d) The simplified mode of the 2-D layer with single E and triple E bridges and the bridging water ligands. (e) The unprecedented Nd-oxo cluster chain constituted by $\{Nd_6\}$ rings through sharing the bridging water ligands.

($\{Nd_8Ge_{12}\}$-**6A**) and $[Nd_8Ge_{12}(\mu_3\text{-}O)_{24}E_{12}(H_2O)_{16}]$ ($\{Nd_8Ge_{12}\}$-**6B**) subunits with different spatial orientations are observed in the molecular structural unit (Figure S7 in the Supporting Information). The main differences between $\{Nd_8Ge_{12}\}$-**6A** and $\{Nd_8Ge_{12}\}$-**6B** subunits lie in two aspects: (1) the $\{Nd_8Ge_{12}\}$-**6A** subunit has 10 terminal water ligands, whereas the $\{Nd_8Ge_{12}\}$-**6B** subunit owns 16 terminal water ligands; (2) two Nd^{3+} ions located on two polar positions of the $\{Nd_8Ge_{12}\}$-**6A** subunit adopt nine-coordinate irregular dodecahedra that is similar to that observed in the $\{Pr_8Ge_{12}\}$-**1** SBU, while two Nd^{3+} ions located on two polar positions of the $\{Nd_8Ge_{12}\}$-**6B** subunit dwell in the 10-coordinate distorted hexadecahedra (Figure S8 in the Supporting Information). In the meantime, two $\{Nd_8Ge_{12}\}$-**6A** and $\{\{Nd_8Ge_{12}\}$-**6B** subunits are dimerized together by a bridging water ligand and three carboxylic bridges from three E groups (one is from $\{Nd_8Ge_{12}\}$-**6A** unit, and the other two come from $\{Nd_8Ge_{12}\}$-**6B**), forming the molecular structural unit of **6**, to our knowledge, which represents the largest LnGC SBU to date. Two E groups attached to two Ge centers (Ge9A and Ge12, A: $1-x, 1-y, 1-z$) in the $\{Nd_8Ge_{12}\}$-**6B** subunit not only provide two inflexed carboxylic O atoms to complete the geometry of the $Nd7^{3+}$ ion, but also contribute their extrovertive carboxylic O atoms to participate in the coordination of $Nd4^{3+}$ and $Nd2^{3+}$ ions in the equatorial position of the $\{Nd_8Ge_{12}\}$-**6A** subunit, respectively. In contrast, the $\{Nd_8Ge_{12}\}$-**6A** subunit only donates one E group binding to the Ge3B (B: $-x, -y, -z$) center to chelate the $Nd7^{3+}$ ion in the equatorial position of the $\{Nd_8Ge_{12}\}$-**6B** subunit. In addition, the dihedral angle of two Nd_6 rings encapsulated in $\{Nd_8Ge_{12}\}$-**6A** and $\{Nd_8Ge_{12}\}$-**6B** subunits is 82.6(2)° (Figure 2b), indicating that $\{Nd_8Ge_{12}\}$-**6A** and $\{Nd_8Ge_{12}\}$-**6B** subunits in the molecular structural unit are nearly orthogonal. Above all, **6** exhibits the beautiful 2-D LnGCOL fashion constructed

DOI: 10.1021/acs.inorgchem.6b00754
Inorg. Chem. 2016, 55, 5671–5683

from $\{Nd_8Ge_{12}\}$-**6A** and $\{Nd_8Ge_{12}\}$-**6B** subunits by virtue of E groups and water ligands, which obviously differentiate from the construction of the 1-D LnGCOC arrangement of **1** made up of $\{Pr_8Ge_{12}\}$-**1** subunits by E bridges. As demonstrated in Figure 2c, neighboring $\{Nd_8Ge_{12}\}$-**6A** and $\{Nd_8Ge_{12}\}$-**6B** subunits alternatively interlink together to form 1-D LnGCOC via coordination of three carboxylic groups of three E connectors and one water ligand bridge from the Nd_6 rings encapsulated in $\{Nd_8Ge_{12}\}$-**6A** and $\{Nd_8Ge_{12}\}$-**6B** subunits and then two carboxylic groups of two E groups linking to two Nd^{3+} ions with the opposite direction in the Nd_6 ring from $\{Nd_8Ge_{12}\}$-**6B** subunit are combined with two monocapped Nd^{3+} ions with the opposite direction in the polar positions of the $\{Nd_8Ge_{12}\}$-**6A** subunit, giving rise to the neoteric parallelogram 2-D LnGCOL (Figure 2d). The simplified mode of the quadruple linkages and single linkages are highlighted in Figure 2d. It should be emphasized that the 2-D LnGCOL can be also viewed as an assembly of $\{Nd_8Ge_{12}\}$ SBUs by replacing active water ligands on the $\{Nd_6\}$ rings on the equatorial positions and/or active water ligands on the Nd^{3+} ions on the polar positions of the $\{Nd_8Ge_{12}\}$ SBUs with the O_{COO} atoms from E groups. In the 2-D LnGCOC of **6**, provided that the bridging E groups are removed away, another unprecedented Nd-oxo cluster chain constituted by $\{Nd_6\}$ rings through sharing the bridging water ligands can be found (Figure 2e).

Structures of 2-D LnGCOLs of 7 and 8. When pyridine was replaced by propanedioic acid in the reaction system of **6**, we obtained two 2-D LnGCOLs **7** and **8** $\{[Ln_2GeE(HO)_2O(H_2O)(CH_3COO)_2(CO_3)]_2[Ln_8Ge_{12}E_{12}(\mu_3\text{-}O)_{24}(H_2O)_{10}]\}\cdot 6H_2O$ (Ln^{3+} = Pr^{3+}, **7**; Nd^{3+}, **8**) (Figure 3a and Figure S9 in the Supporting Information) that are remarkably distinct from 2-D COL of **6**. Beyond our expectation, propanedioic acid is transformed to acetate and carbonate to participate in the structural construction of **7** and **8**. Similar decarboxylation has been previously observed.[21a] Furthermore, part $E_2Ge_2O_3^{2-}$ ligands are decomposed to $EGeO_3^{4-}$ ligands to participate in the structural construction of **7** and **8**, and this phenomenon is for the first time encountered. In comparison with **6**, much more negative charge ligands such as CH_3COO^-, CO_3^{2-}, and $EGeO_3^{4-}$ take part in the formation of **7** and **8**, which facilitate more positive Ln^{3+} ions to incorporate into the skeletons of final products. Since **7** and **8** are isomorphic, only **7** is described here. The structural unit of **7** (Figure 3a) contains a cage-like $[Pr_8Ge_{12}E_{12}(\mu_3\text{-}O)_{24}(H_2O)_{10}]$ ($\{Pr_8Ge_{12}\}$-**7**) LnGC (Figure 3b) supported by two unobserved dimeric $\{[Pr_2GeE(HO)_2O(H_2O)(CH_3COO)_2(CO_3)]_2$ fragments (Figure 3c). The major backbone of $\{Pr_8Ge_{12}\}$-**7** is similar to $\{Nd_{16}Ge_{24}\}$-**6B**. In the dimeric $\{[Pr_2GeE(HO)_2O(H_2O)(CH_3COO)_2(CO_3)]$ fragment, the resulting $EGeO_3^{4-}$ moiety not only coordinates to the $Pr4^{3+}$ ion by a O_{COO} atom but also chelates the $Pr5^{3+}$ ion via two hydroxyl oxygen (O_{OH}) atoms from the $\{GeCO(OH)_2\}$ tetrahedron. The two O_{OH} atoms (BVS: 1.08 and 0.94 for O26 and O27) are determined by BVS calculations.[21b−d] Simultaneously, $Pr4^{3+}$ and $Pr5^{3+}$ ions are also joined together by one CH_3COO^- anion and one CO_3^{2-} anion. Two equivalent $\{[Pr_2GeE(HO)_2O(H_2O)(CH_3COO)_2(CO_3)]$ dimeric fragments are symmetrically attached to $Pr2^{2+}$ and $Pr2A^{2+}$ ions on both sides of the $\{Pr_8Ge_{12}\}$-**7** LnGC through the bridging role of two CH_3COO^-, two CO_3^{2-} and two E group from the cage-like $\{Pr_8Ge_{12}\}$-**7**. Notably, in the $\{[Pr_2GeE(HO)_2O(H_2O)(CH_3COO)_2(CO_3)]_2[Pr_8Ge_{12}E_{12}(\mu_3\text{-}O)_{24}(H_2O)_{10}]\}$ SBU, four bidentate μ_2-η^1:η^2 CH_3COO^- and two tridentate μ_3-η^2:η^2:η^2 CO_3^{2-} anions not only stabilize two dimeric $\{[Pr_2GeE(HO)_2O(H_2O)(CH_3COO)_2(CO_3)]$ fragments, but also promote the integration of two $\{[Pr_2GeE(HO)_2O(H_2O)(CH_3COO)_2(CO_3)]$ fragments to the central $\{Pr_8Ge_{12}\}$-**7** LnGC. Although coordination geometries of Pr^{3+} ions (Figure S10a−f in the Supporting Information) in $\{Pr_8Ge_{12}\}$-**7** LnGC are similar to those in $\{Nd_8Ge_{12}\}$-**6B**, coordination environments of Pr^{3+} ions in the dimeric $[Pr_2GeE(HO)_2O(H_2O)(CH_3COO)_2(CO_3)]$ fragment are interesting: (a) the irregular dodecahedral geometry of the $Pr4^{3+}$ ion is defined by two O atoms from one tridentate μ_3-η^2:η^2:η^2 CO_3^{2-} ligand, one O atom from the other tridentate μ_3-η^2:η^2:η^2 CO_3^{2-} ligand, two O atoms from a bidentate μ_2-η^1:η^2 CH_3COO^- anion, one O_{COO} atom and one O_{Ge} from one $EGeO_3^{4-}$ moiety and one O_{COO} atom of $E_2Ge_2O_3^{2-}$ from neighboring $\{Pr_8Ge_{12}\}$-**7** subunit and one water ligand (Figure S10g−i in the Supporting Information); (b) The $Pr5^{3+}$ ion inhabits in a nine-coordinate monocapped square antiprism, which is finished by three O atoms from two bidentate μ_2-η^1:η^2 CH_3COO^- ligands, one O atom from a tridentate μ_3-η^2:η^2:η^2 CO_3^{2-}, two O_{COO} atoms from two $E_2Ge_2O_3^{2-}$ groups, and two O_{Ge} atoms from one $EGeO_3^{4-}$ moiety (Figure S10j−l in the Supporting Information). Interestingly, two dimeric $[Pr_2GeE(HO)_2O(H_2O)(CH_3COO)_2(CO_3)]$ fragments are fused together to form a tetra-Pr^{3+} $[Pr_2GeE(HO)_2O(H_2O)(CH_3COO)_2(CO_3)]_2$ cluster via two CO_3^{2-} linkers (Figure 3d). More intriguingly, $\{Pr_8Ge_{12}\}$-**7** LnGCs and tetra-Pr^{3+} $[Pr_2GeE(HO)_2O(H_2O)(CH_3COO)_2(CO_3)]_2$ clusters are alternately interlinked and generate a 1-D COC assembly (Figure 3e), which is entirely different from the 1-D COC of **6** formed by $\{Nd_8Ge_{12}\}$-**6A** and $\{Nd_8Ge_{12}\}$-**6B** LnGCs via the quadruple linkages (three carboxylic groups of three E connectors and one water ligand). Neighboring 1-D COCs are further joined via singlet carboxyl groups of E groups linking the $Pr3^{3+}$ ions in the equatorial position of $\{Pr_8Ge_{12}\}$-**7** LnGCs and the $Pr5^{3+}$ ions in tetra-Pr^{3+} $[Pr_2GeE(HO)_2O(H_2O)(CH_3COO)_2(CO_3)]_2$ clusters, propagating 2-D COL of **7** (Figure 3f). It should be noted that adjacent 1-D COCs are antiparallel to each other and lie in two planes (Figure 3g). Notably, there are two

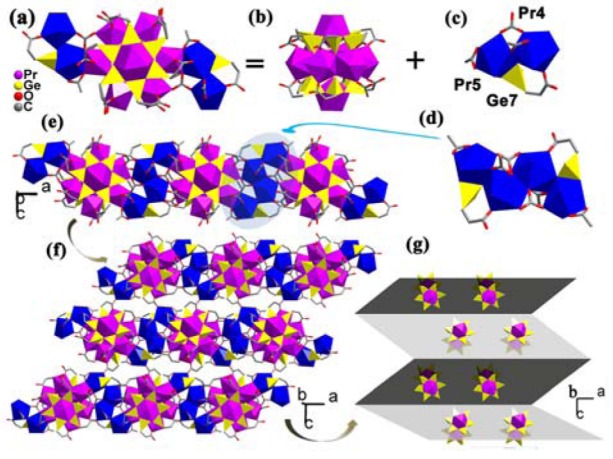

Figure 3. (a) View of $\{[Pr_2Ge(HO)_2O(H_2O)E(CH_3COO)_2(CO_3)]_2[Pr_8Ge_{12}E_{12}(\mu_3\text{-}O)_{24}(H_2O)_{10}]\}$ SBU in **7**. (b) The $\{Pr_8Ge_{12}\}$-**7** subunit. (c) The dimeric $\{[Pr_2Ge(HO)_2O(H_2O)E(CH_3COO)_2(CO_3)]_2$ fragment. (d) The tetra-Pr^{3+} $[Pr_2GeE(HO)_2O(H_2O)(CH_3COO)_2(CO_3)]_2$ cluster. (e) The 1-D chain in **7**. (f) The 2-D layer structure of **7**. (g) Schematic view of the waved 2-D layer.

DOI: 10.1021/acs.inorgchem.6b00754
Inorg. Chem. 2016, 55, 5671−5683

differences between 2-D COLs in **6** and **7**: (a) the 2-D COL of **6** is formed by alternate $\{Nd_8Ge_{12}\}$-**6A**/**6B** LnGCs, whereas the 2-D COL of **7** is built by alternate $\{Pr_8Ge_{12}\}$-**7** LnGCs and $[Pr_2GeE(HO)_2O(H_2O)(CH_3COO)_2(CO_3)]_2$ clusters; (b) the 2-D COL **6** is planar while **7** exhibits a waved 2-D COL. These differences enlighten us to explore whether the introduction of rigid carboxylic ligands will build more intriguing 3-D LnGCOFs established by $\{Nd_8Ge_{12}\}$ subunits and Ln-organic complexes or clusters. On the basis of this synthetic principle, several rigid organic carboxylic ligands (Hpca, Hpza, and H_2pda) were employed, which led to the isolation of the 3-D COFs of **9**−**12**.

Structure of 3-D LnGCOF of 9. The structural unit of **9** (Figure 4a) is formed by two half-units $[TbGeE(HO)_2O(H_2O)(pca)][Tb_4Ge_6E_6(\mu_3\text{-}O)_{12}(H_2O)_4]$ (Figure S11 in the Supporting Information) by an inversion center of (0.5, 0.5, 1). Alternatively, its SBU can be also viewed as a cage-like $[Tb_8Ge_{12}E_{12}(\mu_3\text{-}O)_{24}(H_2O)_8]$ ($\{Tb_8Ge_{12}\}$-**9**) LnGC (Figure 4b) with two supporting $[TbGeE(HO)_2O(H_2O)(pca)]$ fragments (Figure 4c). The skeleton of $\{Tb_8Ge_{12}\}$-**9** is very analogous to $\{Pr_8Ge_{12}\}$-**1** and $\{Nd_8Ge_{12}\}$-**6A** except that some water ligands are substituted by O_{COO} atoms from $E_2Ge_2O_3^{2-}$, $EGeO_3^{4-}$, and pca^- ligands and O_{OH} atoms from $EGeO_3^{4-}$ ligands. In the $[TbGeE(HO)_2O(H_2O)(pca)]$ fragment, the pca^- ligand utilizes the N atom and one O_{COO} atom to coordinate to the $Tb2^{3+}$ ion, and the $EGeO_3^{4-}$ moiety donates a O_{COO} atom and two O_{OH} atoms from the $\{GeCO(OH)_2\}$ tetrahedron to chelate the $Tb2^{3+}$ ion (Figure S12a in the Supporting Information). BVS calculations indicate that the BVS values of two O_{OH} atoms are 1.08 for O26 and 0.94 for O27.[21b−d] Similar to combination of two $[Pr_2GeE(HO)_2O(H_2O)(CH_3COO)_2(CO_3)]$ fragments with the $\{Pr_8Ge_{12}\}$-**7** cage in **7**, two remaining O_{COO} atoms and two remaining O_{Ge} atoms from $EGeO_3^{4-}$ ligands in the $[TbGeE(HO)_2O(H_2O)(pca)]$ fragment substitute four water ligands on the equatorial $Tb4^{3+}$, $Tb4A^{3+}$, $Tb5^{3+}$, and $Tb5A^{3+}$ ions (A: $1-x$, $1-y$, $2-z$) of the central $\{Tb_8Ge_{12}\}$-**9** cage, giving rise to the centrosymmetric $[TbGeE(HO)_2O(H_2O)(pca)]_2[Tb_8Ge_{12}E_{12}(\mu_3\text{-}O)_{24}(H_2O)_8]$ SBU. Meanwhile, water ligands on $Tb2^{3+}$ and $Tb2A^{3+}$ ions are activated and entirely replaced with four extrovertive O_{COO} atoms from E groups, which reinforce the construction of $[TbGeE(HO)_2O(H_2O)(pca)]_2[Tb_8Ge_{12}E_{12}(\mu_3\text{-}O)_{24}(H_2O)_8]$ SBUs. During this process, the eight-coordinate $Tb2^{3+}$ center integrates one extra O_{COO} atom from the E group of adjacent $[TbGeE(HO)_2O(H_2O)(pca)]$ moiety and one atom from water ligand to complete its dodecahedron geometry (Figure S12b-c in the Supporting Information). Notably, adjacent $[TbGeE(HO)_2O(H_2O)(pca)]$ fragments are also dimerized to the di-Tb^{3+} $[TbGeE(HO)_2O(H_2O)(pca)]_2$ cluster (Figure 4d). From the viewpoint of combination chemistry, the alternate connection of the $\{Tb_8Ge_{12}\}$-**9** subunits and di-Tb^{3+} $[TbGeE(HO)_2O(H_2O)(pca)]_2$ clusters via two carboxyl linkers of E groups forms 1-D COC (Figure 4e) and neighboring 1-D COCs are further joined via the carboxyl linkers of E groups, giving rise to 3-D COF (Figure 4f) with elliptical channels (Figure S13 in the Supporting Information). In the 3-D COF, each $[TbGeE(HO)_2O(H_2O)(pca)]_2[Tb_8Ge_{12}E_{12}(\mu_3\text{-}O)_{24}(H_2O)_8]$ SBU connects six same ones via eight E groups in the equatorial and polar positions (Figure 4g). From the topological point of view, the COF of **9** is a six-connected topological framework with the point symbol of $(4^{12}\cdot6^3)$ (Figure 4h).

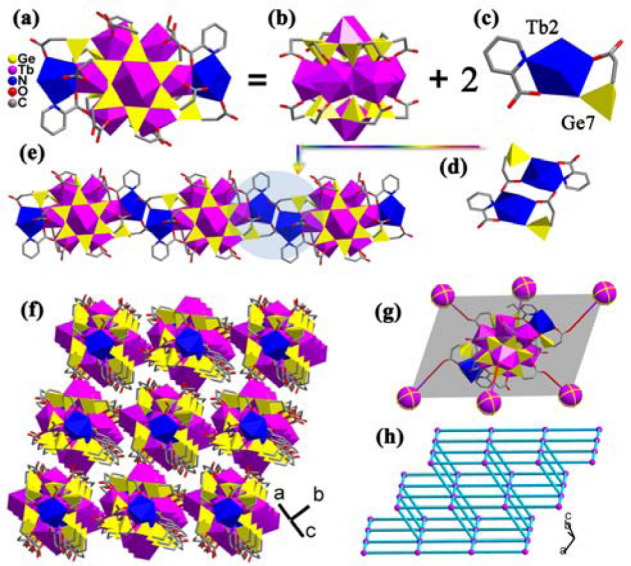

Figure 4. (a) View of the $[TbGeE(HO)_2O(H_2O)(pca)]_2[Tb_8Ge_{12}E_{12}(\mu_3\text{-}O)_{24}(H_2O)_8]$ SBU in **9**. (b) View of the $\{Tb_8Ge_{12}\}$-**9** subunit. (c) View of $[TbGeE(HO)_2O(H_2O)\ (pca)]$ fragment. (d) The di-Tb^{3+} $[TbGeE(HO)_2O(H_2O)(pca)]_2$ cluster. (e) The 1-D chain fashion constructed from $\{Tb_8Ge_{12}\}$-**9** subunits and di-Tb^{3+} $[TbGeE(HO)_2O(H_2O)(pca)]_2$ clusters. (f) The 3-D framework of **9**. (g) The combination mode of each $[TbGeE(HO)_2O(H_2O)(pca)]_2[Tb_8Ge_{12}E_{12}(\mu_3\text{-}O)_{24}(H_2O)_8]$ SBU with six neighboring same SBUs. (h) The topological view of the 3-D framework of **9** (purple nodes represent $[TbGeE(HO)_2O(H_2O)(pca)]_2[Tb_8Ge_{12}E_{12}(\mu_3\text{-}O)_{24}(H_2O)_8]$ SBUs).

Structure of 3-D LnGCOF of 10. **10** crystallizes in the triclinic space group $P\bar{1}$ and demonstrates an unusual 3-D LnGCOF $\{([Nd(pza)_2(H_2O)_2]_2[Nd_8Ge_{12}E_{12}(\mu_3\text{-}O)_{24}(H_2O)_{12}])([Nd(pza)_2]_2[Nd_8Ge_{12}E_{12}(Hpza)_2(\mu_3\text{-}O)_{24}(H_2O)_{10}])\}\cdot4OH\cdot14H_2O$ (Figure 5a, Figure S14 in the Supporting Information), in which two different subunits $\{[Nd(pza)_2(H_2O)_2]_2[Nd_8Ge_{12}E_{12}(\mu_3\text{-}O)_{24}(H_2O)_{12}]\}$ ($\{Nd_{10}Ge_{12}(pza)_4\}$-**10A**) (Figure 5b) and $\{[Nd(pza)_2]_2[Nd_8Ge_{12}E_{12}(Hpza)_2(\mu_3\text{-}O)_{24}(H_2O)_{10}]\}$ ($\{Nd_{10}Ge_{12}(pza)_6\}$-**10B**) (Figure 5c) can be observed. Albeit both $[TbGeE(HO)_2O(H_2O)(pca)]_2[Tb_8Ge_{12}E_{12}(\mu_3\text{-}O)_{24}(H_2O)_8]$ in **9** and $\{Nd_{10}Ge_{12}(pza)_4\}$-**10A** in **10** contain the typical $\{Ln_8Ge_{12}\}$ cage and two additional Ln-organic complex cations, four tridentate pza ligands rather than two $EGeO_3^{4-}$ ligands and two tridentate pca ligands work as stabilizers in the periphery of the $\{Nd_8Ge_{12}\}$ cage in $\{Nd_{10}Ge_{12}(pza)_4\}$ -**10A** unit. The skeleton of $\{Nd_{10}Ge_{12}(pza)_4\}$-**10A** unit can be viewed as a $\{Nd_8Ge_{12}\}$ cage (Figure 5d) linking two $[Nd5(pza)_2(H_2O)_2]^+$ moieties (Figure 5e). The $[Nd5(pza)_2(H_2O)_2]^+$ moiety attaches to the $\{Nd_8Ge_{12}\}$ subunit via two carboxyl groups from two pza ligands and two E groups. The nine-coordinate $Nd5^{3+}$ center (Figure S15a−c in the Supporting Information) binds three extrovertive O_{COO} atoms from two $\{Nd_{10}Ge_{12}(pza)_4\}$-**10A** subunits, two N atoms, and two O_{COO} atoms from two pza ligands and two coordinate water ligands to complete its monocapped square antiprism geometry. Notably, when one terminal water ligand of each capped Nd^{3+} center in the $\{Nd_8Ge_{12}\}$ cage of $\{Nd_{10}Ge_{12}(pza)_4\}$-**10A** unit is replaced by the N atom from a tridentate pza ligand, generating the six-pza-containing $\{Nd_{10}Ge_{12}(pza)_6\}$-**10B** unit that consists of a $\{Nd_8Ge_{12}(Hpza)_2\}$ subunit (Figures 5f and S15d−f in the

DOI: 10.1021/acs.inorgchem.6b00754
Inorg. Chem. 2016, 55, 5671−5683

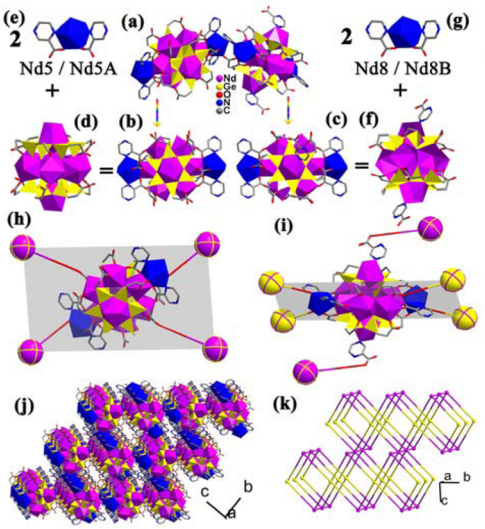

Figure 5. (a) View of the {([Nd(pza)$_2$(H$_2$O)$_2$]$_2$[Nd$_8$Ge$_{12}$E$_{12}$(μ_3-O)$_{24}$(H$_2$O)$_{12}$])([Nd(pza)$_2$]$_2$[Nd$_8$Ge$_{12}$E$_{12}$(Hpza)$_2$(μ_3-O)$_{24}$(H$_2$O)$_{10}$])} SBU in **10**. (b, c) The structures of two different {Nd$_{10}$Ge$_{12}$(pza)$_4$}-**10A** unit and {Nd$_{10}$Ge$_{12}$(pza)$_6$}- **10B** unit. (d, e) The structures of {Nd$_8$Ge$_{12}$} SBU and {Nd(pza)$_2$(H$_2$O)$_2$} moiety in {Nd$_{10}$Ge$_{12}$(pza)$_4$}-**10A**. (f, g) The structures of {Nd$_8$Ge$_{12}$(pza)$_2$} SBU and {Nd(pza)$_2$} moiety in {Nd$_{10}$Ge$_{12}$(pza)$_6$}-**10B**. (h) The **A**(**B**$_4$) four-connected mode of **A**-type {Nd$_{10}$Ge$_{12}$(pza)$_4$}-**10** unit. (i) The **B**(**A**$_4$)(**B**$_2$) six-connected mode of **B**-type {Nd$_{10}$Ge$_{12}$(pza)$_6$}-**10** unit. (j) View of the 3D structure of **10** in the bc plane. (k) Schematic topological view of the 3D framework of **10** (yellow nodes: the {Nd$_{10}$Ge$_{12}$(pza)$_4$}-**10A** units, purple nodes: the {Nd$_{10}$Ge$_{12}$(pza)$_6$}-**10B** units). Blue polyhedral: the Nd^{3+} centers in {Nd(pza)$_2$(H$_2$O)$_2$} and {Nd(pza)$_2$} moieties, Symmetric codes: A: 2 − *x*, − *y*, 1 − *z*.

Supporting Information) and two additional [Nd8(pza)$_2$]$^+$ moieties (Figures 5g and S14g–h in the Supporting Information). The most interesting feature is that each {Nd$_{10}$Ge$_{12}$(pza)$_4$}-**10A** unit joins four {Nd$_{10}$Ge$_{12}$(pza)$_6$}-**10B** units forming a **A**(**B**$_4$) four-connected mode (Figure 5h), whereas each {Nd$_{10}$Ge$_{12}$(pza)$_6$}-**10B** unit is combined with four {Nd$_{10}$Ge$_{12}$(pza)$_4$}-**10A** units and two {Nd$_{10}$Ge$_{12}$(pza)$_6$}-**10B** units creating the **B**(**A**$_4$)(**B**$_2$) six-connected mode (Figure 5i). By this mode, the 3-D COF comes into being (Figure 5j). Topologically, the overall 3-D COF of **10** can be rationalized as a (4,6)-connected net with the point symbol of (4^4·6^2)(4^4·6^{10}·8) (Figure 5k), which is the same to the reported one.[22]

Structures of 3-D LnGCOFs of 11 and 12. {[Nd$_8$Ge$_{12}$E$_{12}$(μ_3-O)$_{24}$(H$_2$O)$_{10}$][Nd(pca)(pda)(H$_2$O)]$_2$}·12H$_2$O (**11**) (Figures 6a and S16 in the Supporting Information) and {[Nd$_8$Ge$_{12}$E$_{12}$(μ_3-O)$_{24}$(H$_2$O)$_{10}$][Nd(pza)(pda)(H$_2$O)]$_2$}·12H$_2$O (**12**) (Figure S17 in the Supporting Information) almost are isostructural and crystallize in the monoclinic space group $P2_1/n$, which display unique 3-D LnGCOFs with dual ligands. The replacement of the pca ligand in the structure of **11** with the pza ligand results in the formation of **12**. Thus, only the structure of **11** is described here. The structural unit of **11** consists of a [Nd$_8$Ge$_{12}$E$_{12}$(μ_3-O)$_{24}$(H$_2$O)$_{10}$] ({Nd$_8$Ge$_{12}$}-**11**) (Figure 6b) subunit and two supporting {Nd(pca)(pda)(H$_2$O)} fragments (Figure 6c). The {Nd$_8$Ge$_{12}$}-**11** subunit is similar to the {Nd$_8$Ge$_{12}$}-**6B** subunit. In the {Nd(pca)(pda)(H$_2$O)} unit, the Nd2^{3+} center is chelated by one N atom and two O$_{COO}$ atoms from a pda ligand, one N atom, and one O$_{COO}$ atom of a pca ligand, three O$_{COO}$ atoms from three E groups and one water ligand (Figure S18 in the Supporting

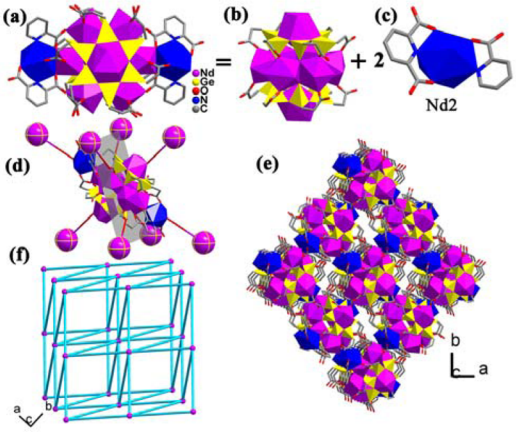

Figure 6. (a) View of {[Nd$_8$Ge$_{12}$E$_{12}$(μ_3-O)$_{24}$(H$_2$O)$_{10}$][Nd(pca)(pda)(H$_2$O)]$_2$} SBU in **11.** (b) View of the {Nd$_8$Ge$_{12}$}-**11** cage. (c) View of the {Nd(pca)(pda)}-**11** moiety. (d) The eight-connected mode of {Nd$_{10}$Ge$_{12}$ (pca) (pda)$_2$}-**11** SBU and the purple balls represent adjacent {Nd$_{10}$Ge$_{12}$(pca)(pda)$_2$}-**11** SBUs. (e) View of the 3D structure of **11** in the *bc* plane. (f) Schematic topological view of the 3D framework of **11** (purple nodes: the {[Nd$_8$Ge$_{12}$E$_{12}$(μ_3-O)$_{24}$(H$_2$O)$_{10}$][Nd(pca)(pda)(H$_2$O)]$_2$} SBUs). Symmetric codes: A: −*x*, 1 − *y*, 1 − *z*.

Information). Moreover, the Nd2^{3+} ion is connected with the equatorial Nd4^{3+} ion in the {Nd$_8$Ge$_{12}$}-**11** subunit through four carboxylic bridges from a pda ligand, a pca ligand, and two E groups. Although the major skeleton of SBU in **11** is similar to the {Nd$_{10}$Ge$_{12}$(pza)$_4$}-**10A** unit accompanying pza ligands replaced by pca and pda ligands, each {Nd$_8$Ge$_{12}$}-**11** subunit utilizes the eight-connected mode (each {Nd$_{10}$Ge$_{12}$(pza)$_4$}-**10A** unit uses the four-connected mode) to link eight adjacent {Nd$_8$Ge$_{12}$}-**11** subunits through four {Nd(pca)(pda)(H$_2$O)} fragments and four E groups (Figure 6d), generating an unobserved 3-D LnGCOF (Figure 6e). Topologically, the LnGCOF of **11** can be considered as an 8-connected net with the point symbol of (4^{24}·6^4) (Figures 6e–f and S19 in the Supporting Information), which is the same to the reported one.[23]

PXRD Patterns and Thermal Stability. In order to identify the phase purity of **1**–**12**, their PXRD patterns have been measured, and the consistency of the PXRD patterns of the bulks and the calculated XRD patterns from the single-crystal structural analyses proves the good phase purity of **1**–**12** (Figures S20–22 in the Supporting Information). For the sake of investigating the thermal stability of **1**–**12**, their TG analyses were investigated in dry air atmosphere from 25 to 1000 °C at a heating rate of 10 °C/min (Figure S23 in the Supporting Information). The TG curves of **1**–**5** show similar two stages of weight loss between 25 and 1000 °C. The first weight loss of 13.86% (calcd. 14.27%) from 25 to 409 °C for **1**, 14.33% (calcd. 14.17%) from 25 to 403 °C for **2**, 13.57% (calcd. 13.99%) from 25 to 399 °C for **3**, 13.72% (calcd. 13.94%) from 25 to 374 °C for **4**, 14.00% (calcd. 13.79%) from 25 to 388 °C for **5** can be assigned to the release of 14 lattice molecules and 16 coordinate water molecules. The second weight loss of 17.29% (calcd. 17.76%) from 409 to 1000 °C for **1**, 17.62% (calcd. 17.64%) from 403 to 1000 °C for **2**, 17.41% (calcd. 17.42%) from 399 to 1000 °C for **3**, 17.50% (calcd. 17.36%) from 374 to 1000 °C for **4**, 17.17% (calcd. 16.90%) from 388 to 1000 °C for **5**, correspond to the departure of the organic components via combustion. The observed residual weights

DOI: 10.1021/acs.inorgchem.6b00754
Inorg. Chem. 2016, 55, 5671–5683

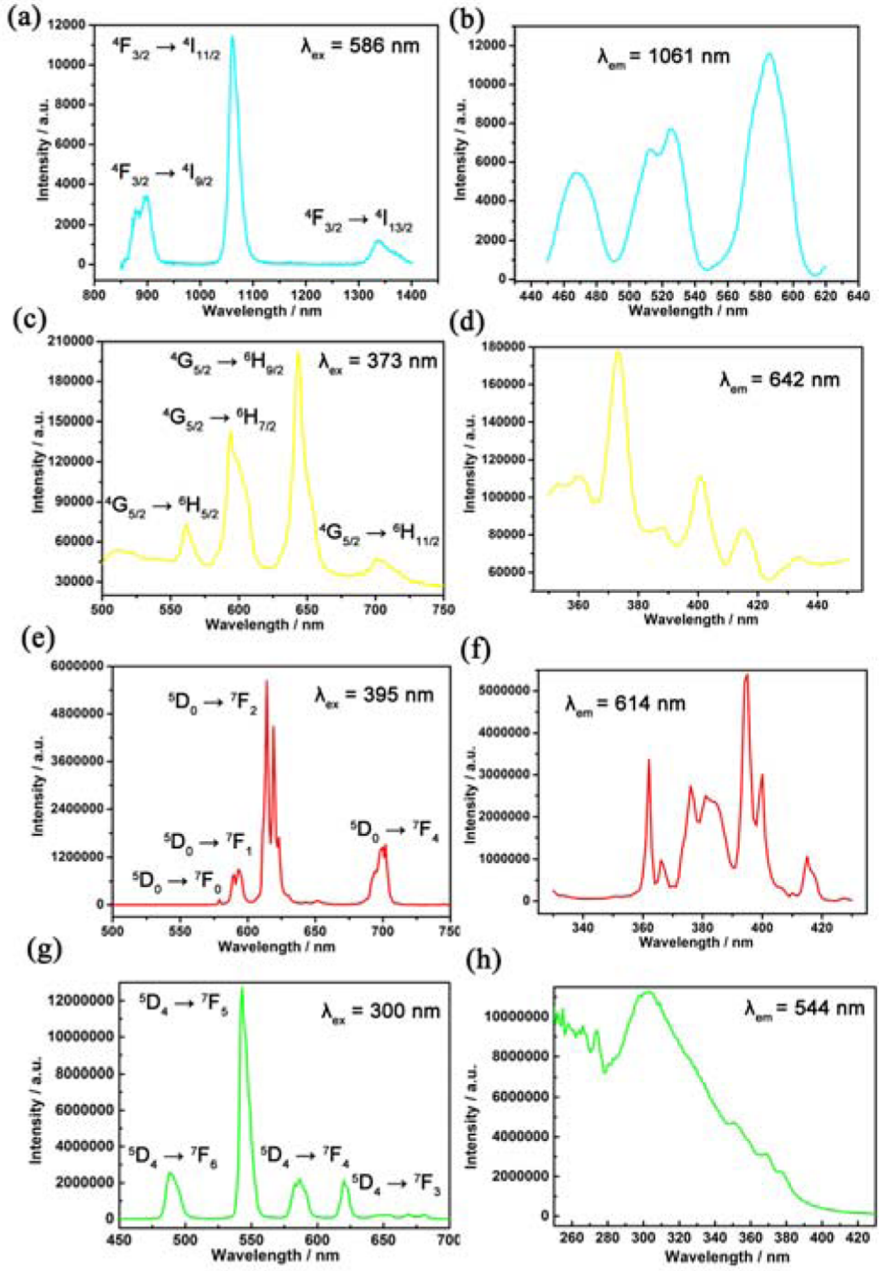

Figure 7. (a) The solid-state emission spectrum of 2 (λ_{ex} = 586 nm) at room temperature. (b) The solid-state excitation spectrum of 2 (λ_{em} = 1061 nm). (c) The solid-state emission spectrum of 3 (λ_{ex} = 373 nm) at room temperature. (d) The solid-state excitation spectrum of 3 (λ_{em} = 642 nm). (e) The solid-state emission spectrum of 4 (λ_{ex} = 395 nm) at room temperature. (f) The solid-state excitation spectrum of 4 (λ_{em} = 614 nm). (g) The solid-state emission spectrum of 9 (λ_{ex} = 300 nm) at room temperature. (h) The solid-state excitation spectrum of 9 (λ_{em} = 544 nm).

(68.85% for **1**, 68.05% for **2**, 69.02% for **3**, 68.78% for **4**, 68.83% for **5**) are in good agreement with the calculated values (67.90% for **1**, 68.21% for **2**, 68.61% for **3**, 68.71% for **4**, 69.05% for **5**), which correspond well to the residues of $4Pr_2O_3 \cdot 12GeO_2$, $4Nd_2O_3 \cdot 12GeO_2$, $4Sm_2O_3 \cdot 12GeO_2$, $4Eu_2O_3 \cdot 12GeO_2$ and $4Gd_2O_3 \cdot 12GeO_2$ for **1**−**5**, respectively. As for **6**, the weight loss before 340 °C is attributed to the liberation of 18 lattice water molecules and 28 coordinated water molecules (observed 11.57%, calcd. 11.23%). Continuous heating to 1000 °C, organic components are combusting with the observed weight loss of 18.22% (calcd. 17.43%). Finally, the main residue is $8Nd_2O_3 \cdot 24GeO_2$ (observed 70.21%, calcd. 70.54%). The total decomposition processes of **7** and **8** are divided into two weight loss steps. The first weight loss of 6.82% (calcd. 6.28%) for **7** from 25 to 338 °C and 7.10% (calcd. 6.22%) for **8** from 25 to 351 °C, involving the release of six lattice water molecules and 11 coordinate water molecules. The second weight loss of 23.56% (calcd. 23.18%) from 338 to 1000 °C for **7** and 22.24% (calcd. 22.99%) from 351 to 1000 °C for **8** correspond to the dehydration of four hydroxylic groups and the removal of organic components. The observed residual weight (69.62% for **7**, 69.91% for **8**) are in good agreement with the calculated values (70.56% for **7**, 70.80% for **8**), which correspond to the residues of **7** and **8** are $6Pr_2O_3 \cdot 14GeO_2$ and $6Nd_2O_3 \cdot 14GeO$, respectively. With regard to **9**, the first weight loss in the range of 25 to 390 °C corresponds to the release of 10 lattice water and 10 coordinate water molecules (observed 7.23%, calcd. 7.66%). The dehydration of four hydroxylic groups and the loss

DOI: 10.1021/acs.inorgchem.6b00754
Inorg. Chem. 2016, 55, 5671−5683

Table 2. Summary of Luminescence Lifetimes of 2, 6, 8, 10, 11, 12 Containing Nd^{3+} Centers, 3 Containing Sm^{3+} Centers, 4 Containing Eu^{3+} Centers and 9 Containing Tb^{3+} Centers Taken by Monitoring Their Corresponding Strongest Emissions

compounds	$\tau_1/\mu s$	A_1	percentage (%)	$\tau_2/\mu s$	A_2	percentage (%)	$\tau/\mu s$
2	1.05	3371.30	21.33	10.38	1251.80	78.67	8.38
6	1.24	4339.32	30.00	11.52	1089.99	70.00	8.44
8	1.22	4721.91	31.22	11.00	1157.27	68.78	7.95
10	1.12	3413.08	24.10	11.20	1075.11	75.90	8.77
11	1.16	3773.05	21.64	10.86	1454.61	78.36	8.76
12	1.17	3407.73	23.56	10.90	1189.15	76.44	8.61
3	3.86	2830.23	35.78	8.79	2233.64	64.22	7.03
4	426.76	4436.81	100.00				
9	888.78	4255.82	100.00				

of organic parts are assigned in the heating range of 390 and 1000 °C with the observed value of 22.00% (calcd. 22.31%). The residue $5Tb_2O_3{\cdot}14GeO_2$ with the total weight of 70.77% is in good agreement with the calculated value of 71.05%. In the case of **10**, the TG curve exhibits two stages of weight loss. The first weight loss of 8.94% (calcd. 8.62%) before 383 °C involves the release of 14 lattice water molecules, four hydroxylic groups, and 26 coordinate water molecules. The second weight loss of 26.98% (calcd. 27.14%) between 383 and 1000 °C is assigned to the loss of the organic parts via combustion. The observed total weight is 64.04% is in agreement with the calculated value 64.25% considering the residue as $10Nd_2O_3{\cdot}24GeO_2$. The TG curves of **11** and **12** exhibit two major weight loss stages. The first weight loss of 9.21% (calcd. 9.46%) for **11** between 25 and 398 °C and 8.63% (calcd. 9.46%) for **12** between 25 and 355 °C corresponds to the release of 12 lattice water and 12 coordinate water molecules. The second weight loss of 25.69% (calcd. 26.24%) for **11** between 398 and 1000 °C, 25.89% (calcd. 26.28%) between 355 and 1000 °C for **12** is assigned to the loss of the organic parts via combustion. The observed total weight (65.10% for **11**, 65.68% for **12**) approximately coincides with the calculated value (64.30% for **11**, 64.28% for **12**) that corresponds to the residues of $5Nd_2O_3{\cdot}12GeO_2$ for **11** and **12**.

Photoluminescence (PL) Properties. Recently, Ln^{3+}-based complexes have attracted increasing interest in various fields in light-emitting diodes, plasma displays, protein recognition, monitoring drug delivery, sensory probes, and NIR-emitting materials,[24] because of the electronic features of Ln^{3+} ions derived from valence shell electrons of $[Xe]4f^n$ (n = 0−14) including the shielding of 4f orbitals by the filled $5s^25p^6$ subshells leading to well-defined absorption and emission bands,[25] and the high color purity.[16b,24d] Thus, the PL properties of solid samples of **2**, **3**, **4**, **6**, and **8**−**12** have been investigated at ambient temperature. Upon excitation at around 586 nm, **2**, **6**, **8**, **10**, **11**, and **12** display the typical Nd^{3+}-centered NIR PL emission spectra (Figures 7a and S24a,c,e,g,i in the Supporting Information). Their PL spectra all display three groups of characteristic emission bands corresponding to the $^4F_{3/2} \rightarrow {}^4I_{9/2}$ (876 and 895 nm for **2**, 878 and 898 nm for **6**, 878 and 898 nm for **8**, 877 and 894 nm for **10**, 880 and 900 nm for **11**, 869 and 903 nm for **12**), $^4F_{3/2} \rightarrow {}^4I_{11/2}$ (1061 nm for **2**, 1061 nm for **6**, 1060 nm for **8**, 1059 nm for **10**, 1063 nm for **11**, 1051 nm for **12**) and $^4F_{3/2} \rightarrow {}^4I_{13/2}$ (1333 nm for **2**, 1334 nm for **6**, 1329 nm for **8**, 1325 nm for **10**, 1335 nm for **11**, 1320 nm for **12**) transitions of Nd^{3+} ions.[26] By monitoring the most strong $^4F_{3/2} \rightarrow {}^4I_{11/2}$ emission at 1059 nm for **2**, 1061 nm for **6**, 1060 nm for **8**, 1059 nm for **10**, 1063 nm for **11** and 1051 nm for **12**, their excitation spectra were also collected (Figures 7b and S24b,d,f,h,j in the Supporting Information). Their luminescence decay curves (Figure S25a−f in the Supporting Information) were collected by monitoring the strongest emission and can be fitted to a double exponential function as $I = A_1 \exp(-t/\tau_1) + A_2 \exp(-t/\tau_2)$ (where τ_1 and τ_2 are the fast and slow components of the luminescence lifetimes and A_1 and A_2 are the pre-exponential factors), providing the luminescence lifetimes τ_1 and τ_2 of 1.05 μs (21.33%) and 10.38 μs (78.67%) for **2**, 1.24 μs (30.00%) and 11.52 μs (70.00%) for **6**, 1.22 μs (31.22%) and 11.00 μs (68.78%) for **8**, 1.12 μs (24.10%) and 11.20 μs (75.90%) for **10**, 1.16 μs (21.64%) and 10.86 μs (78.36%) for **11**, and 1.17 μs (23.56%) and 10.90 μs (76.44%) for **12**, respectively. Therefore, based on $\tau = (B_1\tau_1^2 + B_2\tau_2^2)/(B_1\tau_1 + B_2\tau_2)$,[27] their average lifetimes are 8.38 μs for **2**, 8.44 μs for **6**, 7.95 μs for **8**, 8.77 μs for **10**, 8.76 μs for **11**, and 8.61 μs for **12**, respectively (Table 2).

Excitation of the as-synthesized solid of **3** at 373 nm reveals four characteristic luminescent emission bands centered at 561, 594, 642, and 701 nm (Figure 7c), which are respectively attributed to the $^4G_{5/2}$ excited state to the lower ^6H_J levels of the Sm^{3+} ions, namely, the $^4G_{5/2} \rightarrow {}^6H_{5/2}$, $^4G_{5/2} \rightarrow {}^6H_{7/2}$, $^4G_{5/2} \rightarrow {}^6H_{9/2}$, and $^4G_{5/2} \rightarrow {}^6H_{11/2}$ transitions.[28] The most intense peak of $^4G_{5/2} \rightarrow {}^6H_{9/2}$ transition appears at 642 nm and results in an orange yellow luminescence. By monitoring the $^4G_{5/2} \rightarrow {}^6H_{9/2}$ emission at 642 nm, the excitation spectrum of **3** is also collected (Figure 7d). The luminescence decay curve was measured by monitoring the strongest emission (Figure S25g in the Supporting Information), which can be well fitted to a double exponential function, affording τ_1 and τ_2 of 3.86 μs (35.78%) and 8.79 μs (64.22%) and the average lifetime of 7.03 μs (Table 2).

The as-synthesized solid sample of **4** exhibits the red photoluminescence under excitation at 395 nm. The emission spectrum consists of five emission bands (Figure 7e), which correspond to the $^5D_0 \rightarrow {}^7F_0$ (579 nm), $^5D_0 \rightarrow {}^7F_1$ (590 and 593 nm), $^5D_0 \rightarrow {}^7F_2$ (614 and 619 nm), $^5D_0 \rightarrow {}^7F_3$ (651 nm), and $^5D_0 \rightarrow {}^7F_4$ (699 and 702 nm) transitions of the Eu^{3+} ions, respectively.[29] Evidently, the Stark splitting in some emission bands is observed owing to the effect of the ligand field. It is well-known that the $^5D_0 \rightarrow {}^7F_1$ transition is a magnetic dipole transition and insensitive to the local environment whereas the $^5D_0 \rightarrow {}^7F_2$ transition is an electric dipole transition and sensitive to the local environment.[30] In general, the magnetic dipole transitions are parity-allowed and the electric dipole transitions are parity-forbidden. However, when the Ln cations are embedded in the ligand field, non-centrosymmetric interactions permit the mixing of electronic states of opposite parity into the 4f wave functions, therefore, the electric dipole transitions become partly allowed and the intensities of some of these transitions are highly susceptive to the local micro-

DOI: 10.1021/acs.inorgchem.6b00754
Inorg. Chem. 2016, 55, 5671−5683

environment changes of the Ln cations, thereby, the luminescence spectra of Ln cations can offer useful information about their local microenvironments.[24c] In this respect, the luminescence of the Eu^{3+} cation is very suitable to function as a structural probe to detect the coordination symmetry and even the number of aqueous ligands. Particularly, the emission intensity ratio of the $^5D_0 \rightarrow {}^7F_2/{}^5D_0 \rightarrow {}^7F_1$ transitions is hypersensitive to the coordination symmetry of the Eu^{3+} cation and usually utilized as a criterion to decipher the local symmetry of the Eu^{3+} cation.[24c,31] The emission intensity ratio of the $^5D^0 \rightarrow {}^7F_2/{}^5D_0 \rightarrow {}^7F_1$ is 5.2 in **4**, manifesting that the Eu^{3+} cations dwell in the lower symmetric ligand field, which inosculates with the eight-coordinate distorted bicapped trigonal prism geometries of the Eu^{3+} centers in the Eu_6 ring in the equatorial position of the $\{Eu_8Ge_{12}\}$-**4** SBU and the nine-coordinate distorted irregular dodecahedra of the Eu^{3+} centers in the monocapped hexagon $\{EuGe_6\}$ subunits in the polar positions of the $\{Eu_8Ge_{12}\}$-**4** SBU. Monitoring the $^5D_0 \rightarrow {}^7F_2$ emission of Eu^{3+} cation at 614 nm, the excitation spectrum has also been collected (Figure 7f). The lifetime curve of **4** was performed under the most intense emission at 614 nm ($^5D_0 \rightarrow {}^7F_2$) and the excitation at 395 nm (Figure S25h in the Supporting Information), which can be fitted to a single exponential function [$I = A \exp(-t/\tau)$], yielding a lifetime value (τ) of 426.76 μs and the pre-exponential factor (A) of 4436.81 (Table 2).

The solid-state sample of **9** emits green luminescence upon excitation at 300 nm. The emission spectrum displays four obvious characteristic emission peaks at 487, 544, 586, and 620 nm (Figure 7g), which are respectively attributed to the $^5D_4 \rightarrow {}^7F_6$, $^5D_4 \rightarrow {}^7F_5$, $^5D_4 \rightarrow {}^7F_4$, and $^5D_4 \rightarrow {}^7F_3$ transitions of the Tb^{3+} ions.[32] The excitation spectrum of **9** is also obtained by monitoring the most strong emission at 544 nm of the Tb^{3+} cations (Figure 7h). The luminescence decay curve of **9** was also examined under the most intense emission at 544 nm and the excitation at 300 nm (Figure S25i in the Supporting Information), which can also be fitted into a single-exponential function, generating the lifetime of 888.78 μs and a pre-exponential factor (A) of 4255.82 (Table 2).

A better understanding of the trueness of color is highly crucial in the applications of lighting and display devices. Figure 8 shows the CIE chromaticity diagram for **3**, **4**, and **9**. The CIE chromaticity coordinates for **3**, **4**, and **9** are determined on the basis of their corresponding PL spectra and are calculated as (0.48597, 0.49316) for **3**, (0.66161, 0.33806) for **4**, and (0.33701, 0.58897) for **9**.

CONCLUSION

In conclusion, by introducing the second auxiliary ligands to the organogermanate−lanthanide−oxide reaction system, we made six series of novel LnGs **1**−**12** from 1-D LnG COCs, 2-D LnG COLs to 3-D LnG COFs, which are constructed from $\{Ln_8Ge_{12}\}$ clusters via Ln−organic complexes or organic ligand connectors. The structural assembly of **1**−**12** can be imagined as the gradual substitution of active water sites located at equatorial and polar positions on the hypothetical $[Ln_8Ge_{12}(\mu_3\text{-}O)_{24}E_{12}(H_2O)_{18}]$ cluster core by the oxygen atoms from E groups on organogermanium ligands and oxygen and nitrogen atoms from the second auxiliary ligands. It should be pointed out that carboxylate groups from organic ligands play an important role in the construction of extended structures with different topologies. The successful preparations of these LnG

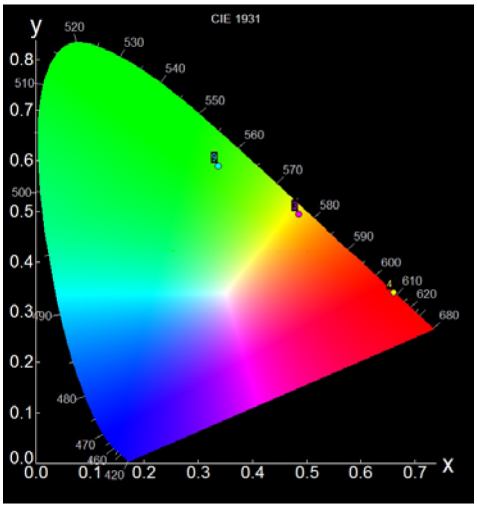

Figure 8. Corresponding color coordinates of 3, 4, and 9 under excitation at 373, 395, and 300 nm, respectively.

COCs/COLs/COFs not only provide a new paradigm for the designed assembly of novel LnGCs via the hydrothermal synthetic strategy, but also open the avenue to profoundly understand and continuously explore the field of the rare-earth organogermanate chemistry. Further work is in progress.

ASSOCIATED CONTENT

Supporting Information

The Supporting Information is available free of charge on the ACS Publications website at DOI: 10.1021/acs.inorgchem.6b00754.

Related structural figures; related PXRD patterns and TG curves of **1**−**12**; the emission and excitation spectra of **6**, **8**, **10**, **11**, and **12** (PDF)

Crystallographic information files (CIF1, CIF2, CIF3, CIF4, CIF5, CIF6, CIF7, CIF8, CIF9, CIF10, CIF11, and CIF12)

AUTHOR INFORMATION

Corresponding Authors

*(G.-Y.Y.) E-mail: ygy@bit.edu.cn. Fax: +86-10-68918572.

*(J.-W.Z.) E-mail: zhaojunwei@henu.edu.cn. Fax: +86-371-23881589.

Author Contributions

#L.-L.L. and G.-J.C. have equal contributions.

Notes

The authors declare no competing financial interest.

ACKNOWLEDGMENTS

This work was supported by the NSFC (Nos. 21571016 and 91122028), and the NSFC for Distinguished Young Scholars (No. 20725101).

REFERENCES

(1) (a) Corma, A. *Chem. Rev.* **1997**, *97*, 2373. (b) Smith, J. V. *Chem. Rev.* **1988**, *88*, 149. (c) Cundy, C. S.; Cox, P. A. *Chem. Rev.* **2003**, *103*, 663.

(2) Liu, G.-Z.; Zheng, S.-T.; Yang, G.-Y. *Angew. Chem., Int. Ed.* **2007**, *46*, 2827.

(3) (a) Cheng, J.; Xu, R. *J. Chem. Soc., Chem. Commun.* **1991**, 483. (b) Cheng, J.; Xu, R.; Yang, G. *J. Chem. Soc., Dalton Trans.* **1991**, 1537.

DOI: 10.1021/acs.inorgchem.6b00754
Inorg. Chem. 2016, 55, 5671−5683

(4) (a) Li, Y.; Zou, X. *Angew. Chem., Int. Ed.* **2005**, *44*, 2012. (b) Castaneda, R.; Corma, A.; Fornes, V.; Rey, F.; Rius, J. *J. Am. Chem. Soc.* **2003**, *125*, 7820. (c) Corma, A.; Rey, F.; Valencia, S.; Jorda, J. L.; Rius, J. *Nat. Mater.* **2003**, *2*, 493. (d) Feng, P.; Bu, X.; Stucky, G. D. *Chem. Mater.* **1999**, *11*, 3025. (e) Cascales, C.; Gutierrez-Puebla, E.; Iglesias, M.; Monge, M. A.; Ruiz-Valero, C. *Angew. Chem., Int. Ed.* **1999**, *38*, 2436. (f) O'Keeffe, M.; Yaghi, O. M. *Chem. - Eur. J.* **1999**, *5*, 2796. (g) Corma, A.; Diaz-Cabanas, M. J.; Martinez-Triguero, J.; Rey, F.; Rius, J. *Nature* **2002**, *418*, 514.

(5) (a) PléVert, J.; Gentz, T. M.; Laine, A.; Li, H.; Young, V. G.; Yaghi, O. M.; O'Keeffe, M. A. *J. Am. Chem. Soc.* **2001**, *123*, 12706. (b) PléVert, J.; Gentz, T. M.; Groy, T. L.; O'Keeffe, M.; Yaghi, O. M. *Chem. Mater.* **2003**, *15*, 714. (c) Liu, G. Z.; Zhang, H. X.; Lin, Z. E.; Zheng, S. T.; Zhang, J.; Zhao, J. T.; Wang, G. M.; Yang, G. Y. *Chem. - Asian J.* **2007**, *2*, 1230. (d) Pan, Q.; Li, J.; Ren, X.; Wang, Z.; Li, G.; Yu, J.; Xu, R. *Chem. Mater.* **2008**, *20*, 370. (e) Pan, Q.; Li, J.; Christensen, K. E.; Bonneau, C.; Ren, X.; Shi, L.; Sun, J.; Zou, X.; Li, G.; Yu, J.; Xu, R. *Angew. Chem., Int. Ed.* **2008**, *47*, 7868. (f) Shi, L.; Bonneau, C.; Li, Y.; Sun, J.; Yue, H.; Zou, X. *Cryst. Growth Des.* **2008**, *8*, 3695. (g) Ren, X.; Li, Y.; Pan, Q.; Yu, J.; Xu, R.; Xu, Y. *J. Am. Chem. Soc.* **2009**, *131*, 14128.

(6) (a) Li, H.; Yaghi, O. M. *J. Am. Chem. Soc.* **1998**, *120*, 10569. (b) Medina, M. E.; Iglesias, M.; Monge, M. A.; Gutiérrez-Puebla, E. *Chem. Commun.* **2001**, 2548. (c) Villaescusa, L. A.; Lightfoot, P.; Morris, R. E. *Chem. Commun.* **2002**, 2220. (d) Villaescusa, L. A.; Wheatley, P. S.; Morris, R. E.; Lightfoot, P. *Dalton Trans.* **2004**, 820. (e) Lin, Z. E.; Zheng, S. T.; Yang, G. Y. *Z. Anorg. Allg. Chem.* **2006**, *632*, 354. (f) Tang, L.; Shi, L.; Bonneau, C.; Sun, J.; Yue, H.; Ojuva, A.; Lee, B. L.; Kritikos, M.; Bell, R. G.; Bacsik, Z.; Mink, J.; Zou, X. *Nat. Mater.* **2008**, *7*, 381.

(7) (a) Li, H.; Eddaoudi, M.; Yaghi, O. M. *Angew. Chem., Int. Ed.* **1999**, *38*, 653. (b) Bu, X.; Feng, P.; Stucky, G. D. *Chem. Mater.* **2000**, *12*, 1505. (c) Bu, X.; Feng, P.; Stucky, G. D. *Chem. Mater.* **2000**, *12*, 1811. (d) Zhou, Y.; Zhu, H.; Chen, Z.; Chen, M.; Xu, Y.; Zhang, H.; Zhao, D. *Angew. Chem., Int. Ed.* **2001**, *40*, 2166. (e) Medina, M. E.; Iglesias, M.; Snejko, N.; GutiéRrez-Puebla, E.; Monge, M. A. *Chem. Mater.* **2004**, *16*, 594.

(8) (a) Medina, M. E.; Gutiérrez-Puebla, E.; Monge, M. A.; Snejko, N. *Chem. Commun.* **2004**, 2868. (b) Zou, X.; Conradsson, T.; Klingstedt, M.; Dadachov, M. S.; O'keeffe, M. *Nature* **2005**, *437*, 716. (c) Christensen, K. E.; Bonneau, C.; Gustafsson, M.; Shi, L.; Sun, J.; Grins, J.; Jansson, K.; Sbille, I.; Su, B. L.; Zou, X. *J. Am. Chem. Soc.* **2008**, *130*, 3758.

(9) Lin, Z. E.; Zhang, J.; Zhao, J. T.; Zheng, S. T.; Pan, C. Y.; Wang, G. M.; Yang, G. Y. *Angew. Chem., Int. Ed.* **2005**, *44*, 6881.

(10) Li, H.; Eddaoudi, M.; Richardson, D. A.; Yaghi, O. M. *J. Am. Chem. Soc.* **1998**, *120*, 8567.

(11) Lin, Z. E.; Zheng, S. T.; Yang, G. Y. *Z. Anorg. Allg. Chem.* **2006**, *632*, 354.

(12) Zhou, Y.; Zhu, H.; Chen, Z.; Chen, M.; Xu, Y.; Zhang, H.; Zhao, D. *Angew. Chem., Int. Ed.* **2001**, *40*, 2166.

(13) (a) Lin, Z. E.; Zhang, J.; Yang, G. Y. *Inorg. Chem.* **2003**, *42*, 1797. (b) Zhang, H. X.; Zhang, J.; Zheng, S. T.; Wang, G. M.; Yang, G. Y. *Inorg. Chem.* **2004**, *43*, 6148. (c) Zhang, H. X.; Zhang, J.; Zheng, S. T.; Yang, G. Y. *Inorg. Chem.* **2005**, *44*, 1166. (d) Wang, G. M.; Sun, Y. O.; Yang, G. Y. *Cryst. Growth Des.* **2005**, *5*, 313. (e) Bu, X.; Feng, P.; Gier, T. E.; Zhao, D.; Stucky, G. D. *J. Am. Chem. Soc.* **1998**, *120*, 13389. (f) Johnson, G. M.; Tripathi, A.; Parise, J. B. *Chem. Mater.* **1999**, *11*, 10. (g) Tang, L.; Dadachov, M. S.; Zou, X. D. *Chem. Mater.* **2005**, *17*, 2530. (h) Pitzschke, D.; Bensch, W. *Angew. Chem., Int. Ed.* **2003**, *42*, 4389. (i) Liu, G. Z.; Zheng, S. T.; Yang, G. Y. *Angew. Chem., Int. Ed.* **2007**, *46*, 2827. (j) Ke, Y. X.; Li, J. M.; Zhang, Y. G.; Lu, S. M.; Lei, Z. B. *Solid State Sci.* **2002**, *4*, 803.

(14) (a) Whitfield, T.; Wang, X.; Jacobson, A. J. *Inorg. Chem.* **2003**, *42*, 3728. (b) Liu, Y.; Yang, X. L.; Zhang, J.; Li, Y. Z.; Du, H. B.; You, X. Z.; Song, Y. *Chem. Commun.* **2008**, 3145. (c) Reisner, B. A.; Tripathi, A.; Parise, J. B. *J. Mater. Chem.* **2001**, *11*, 887. (d) Li, H.; Eddaoudi, M.; Plevert, J.; O'Keeffe, M.; Yaghi, O. M. *J. Am. Chem. Soc.* **2000**, *122*, 12409. (e) Plevert, J.; Sanchez-Smith, R.; Gentz, T. M.; Li, H.; Groy, T. L.; Yaghi, O. M.; O'Keeffe, M. *Inorg. Chem.* **2003**, *42*, 5954. (f) Liu, Z. C.; Weng, L. H.; Chen, Z. X.; Zhao, D. Y. *Inorg. Chem.* **2003**, *42*, 5960. (g) Francis, R. J.; Jacobson, A. J. *Chem. Mater.* **2001**, *13*, 4676. (h) Francis, R. J.; Jacobson, A. J. *Angew. Chem., Int. Ed.* **2001**, *40*, 2879. (i) Liu, Y.; Yang, X. L.; Zhang, J.; Li, Y. Z.; Wang, G.-L.; Du, H. B.; You, X. Z. *J. Solid State Chem.* **2008**, *181*, 2542.

(15) He, H.; Cao, G. J.; Zheng, S. T.; Yang, G. Y. *J. Am. Chem. Soc.* **2009**, *131*, 15588.

(16) (a) Armelao, L.; Quici, S.; Barigelletti, F.; Accorsi, G.; Bottaro, G.; Cavazzini, M.; Tondello, E. *Coord. Chem. Rev.* **2010**, *254*, 487. (b) Bunzli, J. C. G.; Piguet, C. *Chem. Soc. Rev.* **2005**, *34*, 1048.

(17) (a) Ananias, D.; Paz, F. A. A.; Yufit, D. S.; Carlos, L. D.; Rocha, J. *J. Am. Chem. Soc.* **2015**, *137*, 3051. (b) Wang, X.; Li, J. Y.; Han, Y. D.; Li, Y.; Yu, J. H.; Xu, R. R. *Chem. Mater.* **2011**, *23*, 2842. (c) Evans, R. C.; Carlos, L. D.; Douglas, P.; Rocha, J. *J. Mater. Chem.* **2008**, *18*, 1100. (d) Zhao, X. G.; Li, J. Y.; Chen, P.; Li, Y.; Chu, Q. X.; Liu, X. Y.; Yu, J. H.; Xu, R. R. *Inorg. Chem.* **2010**, *49*, 9833.

(18) (a) Sun, Y.-Q.; Zhang, J.; Chen, Y.-M.; Yang, G.-Y. *Angew. Chem., Int. Ed.* **2005**, *44*, 5814. (b) Zhang, M.-B.; Zhang, J.; Zheng, S.-T.; Yang, G.-Y. *Angew. Chem., Int. Ed.* **2005**, *44*, 1385. (c) Cheng, J.-W.; Zhang, J.; Zheng, S.-T.; Zhang, M.-B.; Yang, G.-Y. *Angew. Chem., Int. Ed.* **2006**, *45*, 73.

(19) Tsutsui, M.; Kakimoto, N.; Axtell, D. D.; Oikawa, H.; Asai, K. *J. Am. Chem. Soc.* **1976**, *98*, 8287.

(20) (a) Sheldrick, G. M. *SHELXL97, Program for Crystal Structure Refinement*; University of Gőtingen: Gőtingen, Germany, 1997. (b) Sheldrick, G. M. *SHELXS97, Program for Crystal Structure Solution*; University of Göttingen: Göttingen, Germany, 1997.

(21) (a) Gomez Torres, S.; Meyer, G. *Z. Anorg. Allg. Chem.* **2008**, *634*, 231. (b) Brown, I. D.; Altermatt, D. *Acta Crystallogr., Sect. B: Struct. Sci.* **1985**, *41*, 244. (c) Trzesowska, A.; Kruszynski, R.; Bartczak, T. J. *Acta Crystallogr., Sect. B: Struct. Sci.* **2004**, *60*, 174. (d) Trzesowska, A.; Kruszynski, R.; Bartczak, T. J. *Acta Crystallogr., Sect. B: Struct. Sci.* **2005**, *61*, 429.

(22) Zhang, Z.; Ma, J. F.; Liu, Y. Y.; Kan, W. Q.; Yang, J. *Cryst. Growth Des.* **2013**, *13*, 4338.

(23) Sun, J. Y.; Wang, L.; Zhang, D. J.; Li, D.; Cao, Y.; Zhang, L. Y.; Zeng, S. L.; Pang, G. S.; Fan, Y.; Xu, J. N.; Song, T. Y. *CrystEngComm* **2013**, *15*, 3402.

(24) (a) Rocha, J.; Carlos, L. D.; Paz, F. A. A.; Ananias, D. *Chem. Soc. Rev.* **2011**, *40*, 926. (b) Carlos, L. D.; Sá Ferreira, R. A.; Bermudez, V. de Z.; Ribeiro, S. J. L. *Adv. Mater.* **2009**, *21*, 509. (c) Cui, Y. J.; Yue, Y. F.; Qian, G. D.; Chen, B. L. *Chem. Rev.* **2012**, *112*, 1126. (d) Li, Y.; Zheng, F. K.; Liu, X.; Zou, W. Q.; Guo, C.; Lu, C. Z.; Huang, J. S. *Inorg. Chem.* **2006**, *45*, 6308. (e) Shinoda, S.; Tsukube, H. *Analyst* **2011**, *136*, 431. (f) Wang, X.-D.; Wolfbeis, O. S.; Meier, R. J. *Chem. Soc. Rev.* **2013**, *42*, 7834. (g) Hemmer, E.; Venkatachalam, N.; Hyodo, H.; Hattori, A.; Ebina, Y.; Kishimoto, H.; Soga, K. *Nanoscale* **2013**, *5*, 11339. (h) Armelao, L.; Quici, S.; Barigelletti, F.; Accorsi, G.; Bottaro, G.; Cavazzini, M.; Tondello, E. *Coord. Chem. Rev.* **2010**, *254*, 487. (i) Hess, B. A.; Kedziorski, A.; Smentek, L.; Bornhop, D. J. *J. Phys. Chem. A* **2008**, *112*, 2397.

(25) (a) Eliseeva, S. V.; Bünzli, J. G. *Chem. Soc. Rev.* **2010**, *39*, 189. (b) Sopasis, G. J.; Orfanoudaki, M.; Zarmpas, P.; Philippidis, A.; Siczek, M.; Lis, T.; O'Brien, J. R.; Milios, C. J. *Inorg. Chem.* **2012**, *51*, 1170.

(26) (a) Eckes, F.; Bulach, V.; Guenet, A.; Strassert, C. A.; Cola, L.; Hosseini, M. *Chem. Commun.* **2010**, *46*, 619. (b) Abdelhameed, R. M.; Carlos, L. D.; Silva, A. M. S.; Rocha, J. *Chem. Commun.* **2013**, *49*, 5019.

(27) Fujii, T.; Kodaira, K.; Kawauchi, O.; Tanaka, N.; Yamashita, H.; Anpo, M. *J. Phys. Chem. B* **1997**, *101*, 10631.

(28) (a) Comby, S.; Scopelliti, R.; Imbert, D.; Charbonnière, L.; Ziessel, R.; Bunzli, J. G. *Inorg. Chem.* **2006**, *45*, 3158. (b) Huang, Y.-G.; Wu, B.-L.; Yuan, D.-Q.; Xu, Y.-Q.; Jiang, F.-L.; Hong, M.-C. *Inorg. Chem.* **2007**, *46*, 1171. (c) Li, H. L.; Yang, W.; Wang, X. H.; Chen, L. J.; Ma, J. R.; Zheng, L. W.; Zhao, J. W. *Cryst. Growth Des.* **2016**, *16*, 108.

(29) (a) Zhao, J. W.; Luo, J.; Chen, L. J.; Yuan, J.; Li, H. Y.; Ma, P. T.; Wang, J. P.; Niu, J. Y. *CrystEngComm* **2012**, *14*, 7981. (b) Xia, J.;

DOI: 10.1021/acs.inorgchem.6b00754
Inorg. Chem. 2016, 55, 5671−5683

Zhao, B.; Wang, H.-S.; Shi, W.; Ma, Y.; Song, H.-B.; Cheng, P.; Liao, D.-Z.; Yan, S.-P. *Inorg. Chem.* **2007**, *46*, 3450.
(30) Xu, Q. H.; Li, L. S.; Liu, X. S.; Xu, R. R. *Chem. Mater.* **2002**, *14*, 549.
(31) Zhang, T.; Spitz, C.; Antonietti, M.; Faul, C. F. J. *Chem. - Eur. J.* **2005**, *11*, 1001.
(32) Sun, L.; Li, Y.; Liang, Z.-Q.; Yu, J.; Xu, R.-R. *Dalton Trans.* **2012**, *41*, 12790.

DOI: 10.1021/acs.inorgchem.6b00754
Inorg. Chem. 2016, 55, 5671−5683